

---

# **State Space Modeling and Power Flow Analysis of Modular Multilevel Converters**

Chen Li

Thesis submitted to the faculty of the Virginia Polytechnic Institute and  
State University in partial fulfillment of the requirements for the degree

of

Master of Science

In

Electrical Engineering

Fred C. Lee Chair

Qiang Li

Rolando Burgos

06/16/2016

Blacksburg, VA

Keywords: Modular Multilevel Converters, Capacitor Voltage Reduction,  
Power Flows Analysis, State Trajectory Analysis

---

# State Trajectory Analysis for Modular Multilevel Converter

Chen Li

(Abstract)

For the future of sustainable energy, renewable energy will need to significantly penetrate existing utility grids. While various renewable energy sources are networked with high-voltage DC grids, integration between these high-voltage DC grids and the existing AC grids is a significant technical challenge. Among the limited choices available, the modular multi-level converter (MMC) is the most prominent interface converter used between the DC and AC grids. This subject has been widely pursued in recent years. One of the important design challenges when using an MMC is to reduce the capacitor size associated with each module. Currently, a rather large capacitor bank is required to store a certain amount of line-frequency related circulating energy. Several control strategies have been introduced to reduce the capacitor voltage ripples by injecting certain harmonic current. Most of these strategies were developed using trial and error and there is a lack of a systematic means to address this issue. Most recently, Yadong Lyu has proposed to control the modulation index in order

---

to reduce capacitor ripples. The total elimination of the unwanted circulating power associated with both the fundamental line frequency and the second-order harmonic was demonstrated, and this resulted in a dramatic reduction in capacitor size. To gain a better understanding of the intricate operation of the MMC, this thesis proposes a state-space analysis technique in the present paper. Combining the power flow analysis with the state trajectory portrayed on a set of two-dimensional state plans, it clearly delineates the desired power transfer from the unwanted circulating energy, thus leading to an ultimate reduction in the circulation energy and therefore the required capacitor volume.

---

## **Acknowledgement**

I would like to express my sincere gratitude and appreciation for my advisor, Professor Fred C. Lee, for his continuous guidance, encouragement and support during my study and research in CPES. Through all the tremendous effort Dr. Lee spent on me, I improved myself greatly in many aspects, and of which the most important part is the working attitude – never stop challenging and improving. All of the training I got will definitely benefit me in my whole life.

I also would like to give specific appreciation to the faculty advisors in the REN group, Dr. Dushan Boroyevich, Dr. Rolando Burgos, and Dr. Qiang Li. Their wisdom, knowledge and guidance greatly benefit my research. And it is an honor for me to have Dr. Rolando Burgos and Dr. Qiang Li as my committee members. I am very thankful to them for all the helps and suggestions.

Many aspects of reported work is the team efforts. I would like to appreciate my previous and current colleagues for their contributions and assistances. It includes Mr. Kai Li, Mr. Yadong Lyu, Mr. Eric Hsieh, Mr. Zhang Wei, Mr. Ruiyang Qin. Without their help and assistances, none of any success of this research can be achieved.

I would also like to appreciate Miss Fan Fan and Miss Keara Axelrod

---

who helped me with my thesis editing and polishing.

I would like to thank colleagues in the renewable energy nano-grid consortium (REN) of CPES. It is my honor to work with these talented, knowledgeable, helpful and dedicated people: Dr. Mingkai Mu, Dr. Zhiyu Shen, Dr. Igor Cvetkovic, Mr. Fang Chen, Mr. Eric Hsieh, Mr. Zhengrong Huang, Mr. Sungjae Ohn, Miss Niloofar Rashdi, Miss Ye Tang, Mr. Wei Zhang, Mr. Jun Wang, Mr. Alinaghi Marzoughi, Dr. Marko Jaksic, Dr. Bo Wen, Dr. Yang Jiao, Mr. Chi Li, Mr. Ruiyang Qin, Mr. Shishuo Zhao. It is my precious memory to work with you in the past three years.

I would also like to thank the wonderful members of the CPES staffs who always give me their kindness help: Ms. Teresa Shaw, Mr. David Gilham, Ms. Linda Gallagher, Ms. Teresa Rose, Ms. Marianne Hawthorne, Ms. Linda Long.

My deepest appreciations go towards my parents Yin Li and Xiaohong Zhao, who have always been there with their love, support, understanding and encouragement

---

# Table of Contents

<b>Chapter 1 Introduction</b> .....	1
<i>1.1. Background and History</i> .....	1
<i>1.2. Modular Multilevel Converter in HVDC</i> .....	7
<i>1.3. Challenges of Modular Multilevel Converter</i> .....	11
<i>1.4. Thesis Outline</i> .....	14
<b>Chapter 2 Basis Working Principle</b> .....	17
<i>2.1 Structure of MMC</i> .....	17
<i>2.2 Pulse Width Modulation for MMC</i> .....	18
<i>2.3 Nearest Level Modulation for MMC</i> .....	20
<i>2.4 Basic control loop for voltage balancing in MMC</i> .....	23
<i>2.5 Simplification of MMC</i> .....	25
<i>2.1 Analysis of simplified MMC circuit</i> .....	31
<b>Chapter 3 State Space Analysis</b> .....	40
<i>3.1 Introduction of State Space Analysis</i> .....	40
<i>3.2 State Trajectory Analysis for Different Control Method</i> .....	46
Example 1: Simple control law .....	46
Example 2: Zero harmonic current .....	49
Example 3: Second-order harmonic current injection .....	54
Example 4: Controlling the modulation index.....	58

---

Example 5: High-frequency injection for three-phase MMC.....	65
<b>Chapter 4 Verification of Concept .....</b>	<b>70</b>
<i>4.1 Concept extension to multi modules .....</i>	<i>70</i>
<i>4.2 Scaled down hardware of MMC.....</i>	<i>73</i>
<b>Chapter 5 Conclusion and Future Work.....</b>	<b>82</b>
<i>5.1 Summary and conclusion .....</i>	<i>82</i>
<i>5.2 Future work.....</i>	<i>83</i>
<b>References .....</b>	<b>85</b>

---

## List of Figures

Fig.1. 1 Total loss vs. distance for DC and AC transmission line.....	3
Fig.1. 2 DC and an AC overhead line.....	4
Fig.1. 3 Combine System for AC and DC Transmission Line.....	5
Fig.1. 4 Structure of Voltage Source Converter .....	6
Fig.1. 5 Structure of MMC AC-DC combined system.....	7
Fig.1. 6 Trans Bay Cable in CA with MMC Technology .....	8
Fig.1. 7 Structure of Modular Multilevel Converter .....	9
Fig.1. 8 Sub-module for MMC from Siemens.....	12
Fig.2. 1 Three phase MMC system.....	17
Fig.2. 2 PWM modulation for MMC with one module per arm .....	19
Fig.2. 3 PWM for multi modules per arm MMC.....	20
Fig.2. 4 working principle of the NLM .....	21
Fig.2. 5 The control diagram of NLM .....	22
Fig.2. 6 The voltage balancing control of NLM.....	22
Fig.2. 7 control diagram for average balance control.....	24
Fig.2. 8 control diagram of individual balance control .....	25
Fig.2. 9 Simulation results of three phase MMC.....	27
Fig.2. 10 Simplified one phase MMC circuit with one module per arm..	30
Fig.2. 11 Replacing switching model with average model in MMC.....	30



---

Fig.2. 12 The average circuit model with current loop .....	31
Fig.2. 13 Simulation results for simple control law .....	34
Fig.2. 14. Power transfer diagram .....	38
Fig.3. 1 3D state space diagram for MMC .....	41
Fig.3. 2 2D state plane projection for MMC .....	41
Fig.3. 3 The state plane trajectory of upper arm current and module voltage .....	43
Fig.3. 4 State trajectory of $i_l$ and $v_{c1}$ with different power rating.....	44
Fig.3. 5 2D state trajectory of the $v_{c1}$ and $v_{c2}$ planes and waveforms.....	45
Fig.3. 6 power flow mapped state trajectory of $i_l$ $v_{c1}$ in example 1 .....	47
Fig.3. 7 power flow mapped state trajectory of $i_l$ $v_{c1}$ in example 1 .....	48
Fig.3. 8 simulation results of MMC with harmonic current elimination .	50
Fig.3. 9 Power transfer diagram for $i_{har}=0$ .....	51
Fig.3. 10 2D state trajectory of $i_l$ and $v_{c1}$ with colored areas for $i_{har}=0$	52
Fig.3. 11 2D state trajectory of $v_{c1}$ and $v_{c2}$ with colored area for $i_{har}=0$ .....	53
Fig.3. 12 simulation results of MMC with 2 <sup>nd</sup> order harmonic injection .	54
Fig.3. 13 Power transfer diagram for second-order current injection .....	56
FIG.3. 14 2D state trajectory of $i_l$ and $v_{c1}$ with colored area representing second-order harmonics .....	57
Fig.3. 15 2D state trajectory of $v_{c1}$ and $v_{c2}$ for second-order current injection.....	58
Fig.3. 16 State plane with changing modulation index .....	59

---

Fig.3. 17 modulation index control realized with full bridge module.....	61
Fig.3. 18 simulation results for modulation index control .....	61
Fig.3. 19. Power transfer diagram for $M = 1.15$ .....	62
Fig.3. 20 2D state trajectory of $i_{l1}$ and $v_{c1}$ for $M = 1.15$ .....	63
Fig.3. 21 2D state trajectory of $v_{c1}$ and $v_{c2}$ with colored area for $M = 1.15$ .....	63
Fig.3. 22 comparison of state trajectory for different control strategies ..	64
Fig.3. 23 Three-phase MMC for high-frequency common-mode voltage injection.....	65
Fig.3. 24 Simulation results of high-frequency common-mode voltage injection.....	67
Fig.3. 25 State trajectory comparison of high-frequency injection and over-modulation .....	68
Fig.3. 26 comparison of high frequency injection, modulation index control and ideal case .....	69
Fig.4. 1 Circuit Structure for MMC with 12 module per arm .....	70
Fig.4. 2 Simulation results for proposed control methods.....	71
Fig.4. 3 summary of voltage ripple of the different control method .....	72
Fig.4. 4 semiconductor loss evaluations .....	73
Fig.4. 5 Structure of Scaled down MMC hardware.....	74
Fig.4. 6 circuit of sub-module power stage .....	75
Fig.4. 7 Picture of one sub-module.....	76
Fig.4. 8 one phase leg of the scaled down hardware MMC .....	77

---

Fig.4. 9 experimental results of example 2 and example 3 .....	78
Fig.4. 10 experimental results of modulation index control method.....	79
Fig.4. 11 Three phase scaled down hardware of MMC .....	80

## **List of Tables**

Table 2. 1 SIMULATION PARAMETERS .....	26
Table 2. 2 SIMULATION PARAMETERS .....	33
Table 2. 3 SUMMARY OF ARM CURRENT AND MODULE POWER.....	38
TABLE 3. 1 POWER TRANSFER FOR $I_{HAR}=0$ .....	52
TABLE 3. 2 POWER TRANSFER FOR SECOND-ORDER CURRENT INJECTION ...	56
Table 3. 3 Power transfer for Modulation Index control .....	62
Table 3. 4 Parameters for High-Frequency Injection.....	66
Table 4. 1 Parameters for simulation with 12 modules per arm.....	71
TABLE 4. 2 PARAMETERS OF SCALED DOWN MMC HARDWARE .....	75
TABLE 4. 3 CONTROLLER TASK .....	80

---

# Chapter 1 Introduction

## *1.1. Background and History*

At the beginning, the transmission and distribution of electrical energy start with direct current. In 1882, a 50-kilometer-long DC transmission line with 2 kilovolts was built between Miesbach and Munich in Germany[1]. At that time, rotating DC machines is the only method to realized conversion between reasonable consumer voltages and higher DC transmission voltages.

In an AC system, voltage conversion is simple. An AC transformer allows high power levels and high insulation level with low loss. Furthermore, a three-phase synchronous generator is superior to a DC generator in every aspect. The AC system soon became the only feasible technology for generation, transmission and distribution of electrical

However, for high voltage application, AC transmission lines have disadvantages, which may compel a change to DC technology[2]:

- i. The transmission capacity and the transmission distance are limited by the inductive and capacitive elements of the overhead lines.

- 
- ii. Direct connection between two AC system with different frequencies is not possible.
  - iii. Direct connection between two AC systems with the same frequency or a new connection within a meshed grid may be impossible due to system instability, to high short-circuit levels or undesirable power flow scenarios

In 1941, the first contract for a commercial HVDC system was signed in Germany: 60 MW were to be supplied to the city of Berlin via an underground cable of 115 km length[1].

The advantages of a DC link over an AC link are[2]:

- i. A DC link allows power transmission between AC networks with different frequencies or networks, which cannot be synchronized.
- ii. Inductive or capacitive parameter does not limit the transmission capacity or the maximum length of a DC overhead line or cable. The conductor cross section is fully utilized because there is no skin effect.

For a given transmission task, feasibility studies are also considered before the final decision on implementation of an HVAC

or HVDC system can be made. Fig.1. 1 shows a typical cost comparison curve between AC and DC transmission considering[1]:

- AC vs. DC line costs
- AC vs. DC station terminal costs
- AC vs. DC capitalized value of losses.

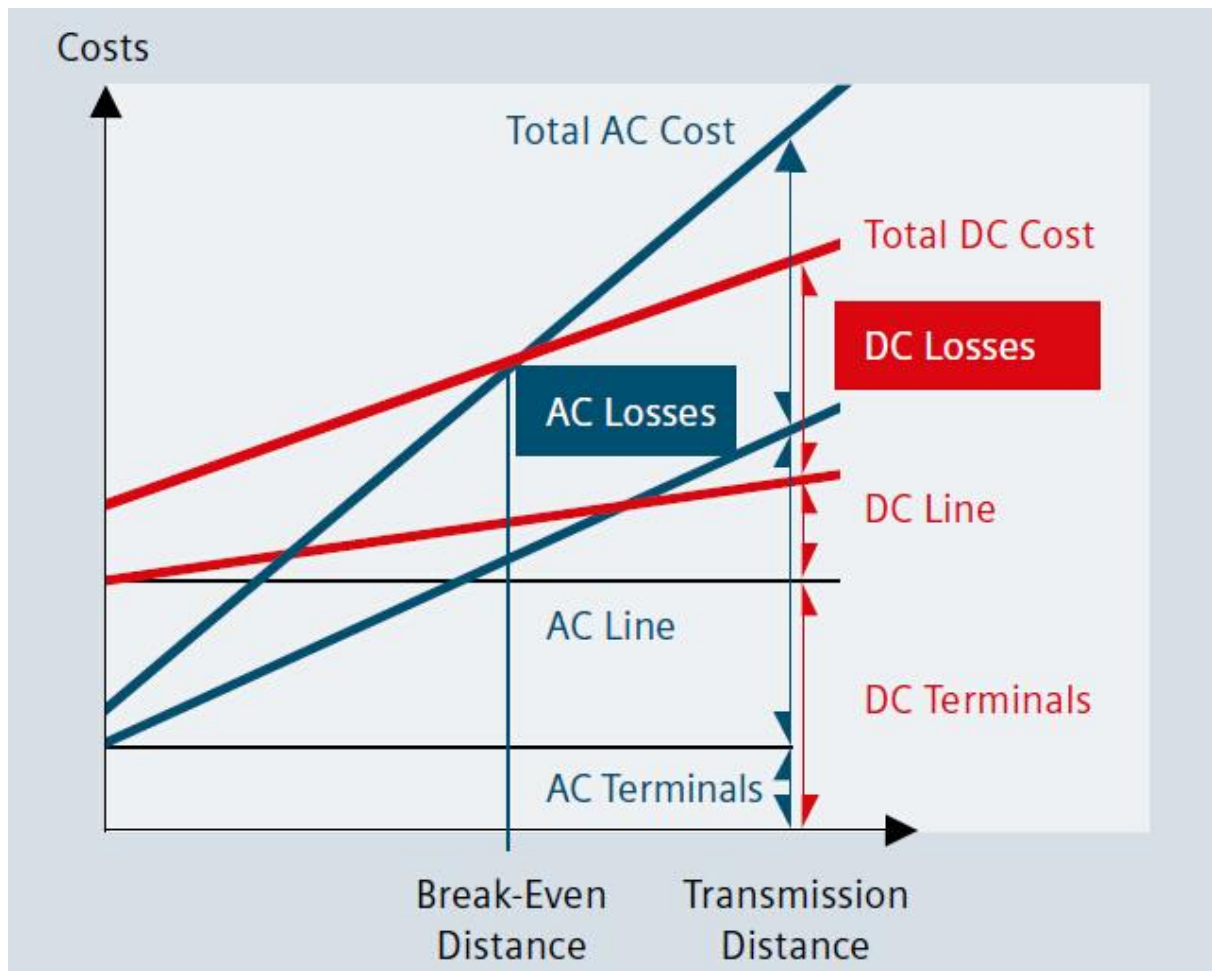


Fig.1. 1 Total loss vs. distance for DC and AC transmission line

---

An HVDC transmission system is also environment friendly because improved energy transmission possibilities contribute to a more efficient utilization of existing power plants

The land coverage and the associated right-of- way cost for an HVDC overhead transmission line is lower. Moreover, it is also possible to increase the power transmission capacity. A comparison between a DC and an AC overhead line is shown in Fig.1. 2[2].

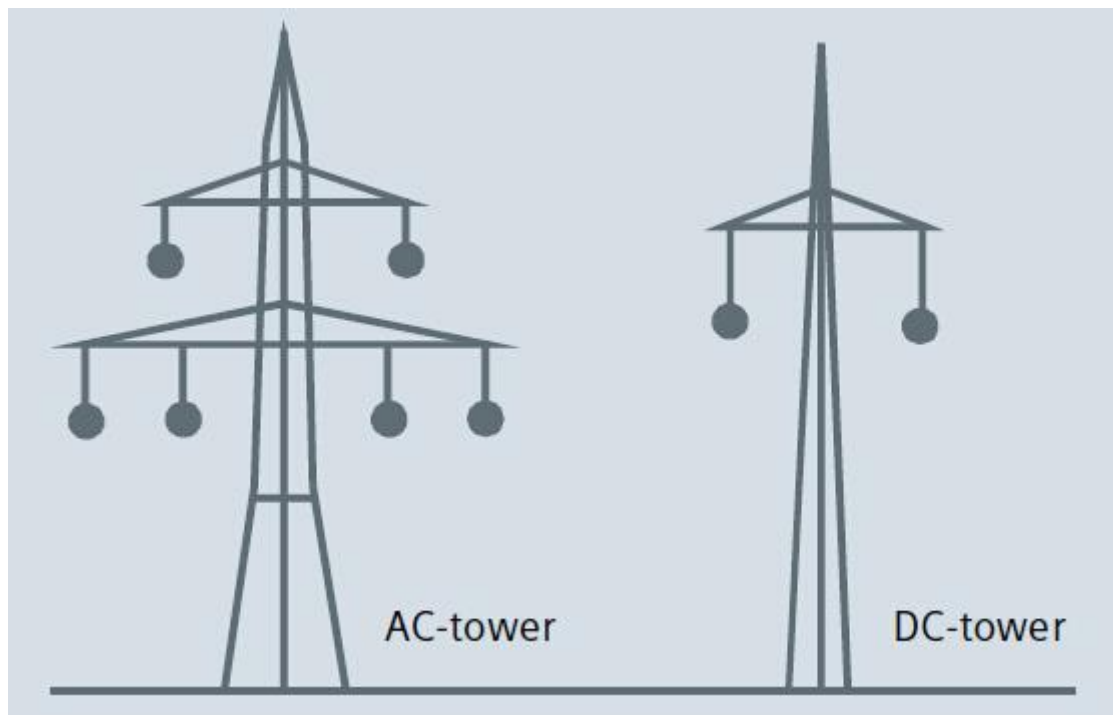


Fig.1. 2 DC and an AC overhead line

Recently, HVDC transmission systems and technologies associated with the flexible ac transmission system (FACTS) continue to advance as they make their way to commercial applications[3][4]. Fig.1. 3 shows the structure of a combine system of HVDC and FACTS. Both HVDC and

FACTS systems underwent research and development for many years, and they were based initially on thyristor technology and more recently on fully controlled semiconductors and voltage-source converter (VSC) topologies[5].

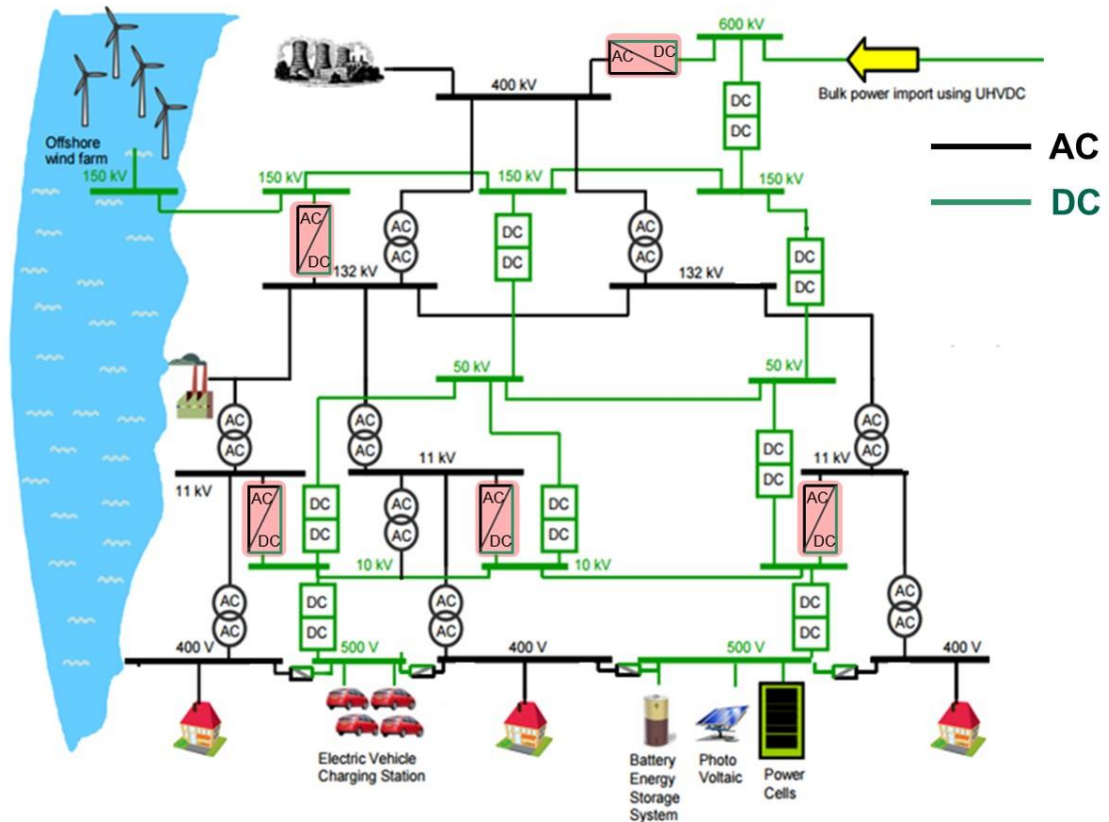


Fig.1. 3 Combine System for AC and DC Transmission Line

Voltage sourced converters require semiconductor devices with turn-off capability. The development of Insulated Gate Bipolar Transistors (IGBT) with high voltage ratings have accelerated the development of voltage sourced converters for HVDC applications in the lower power range[6]. The structure of VSC is in Fig.1. 4 However, the multi-module



VSC-based HVDC converter provides modularity[7], it requires multiple bulky transformers.

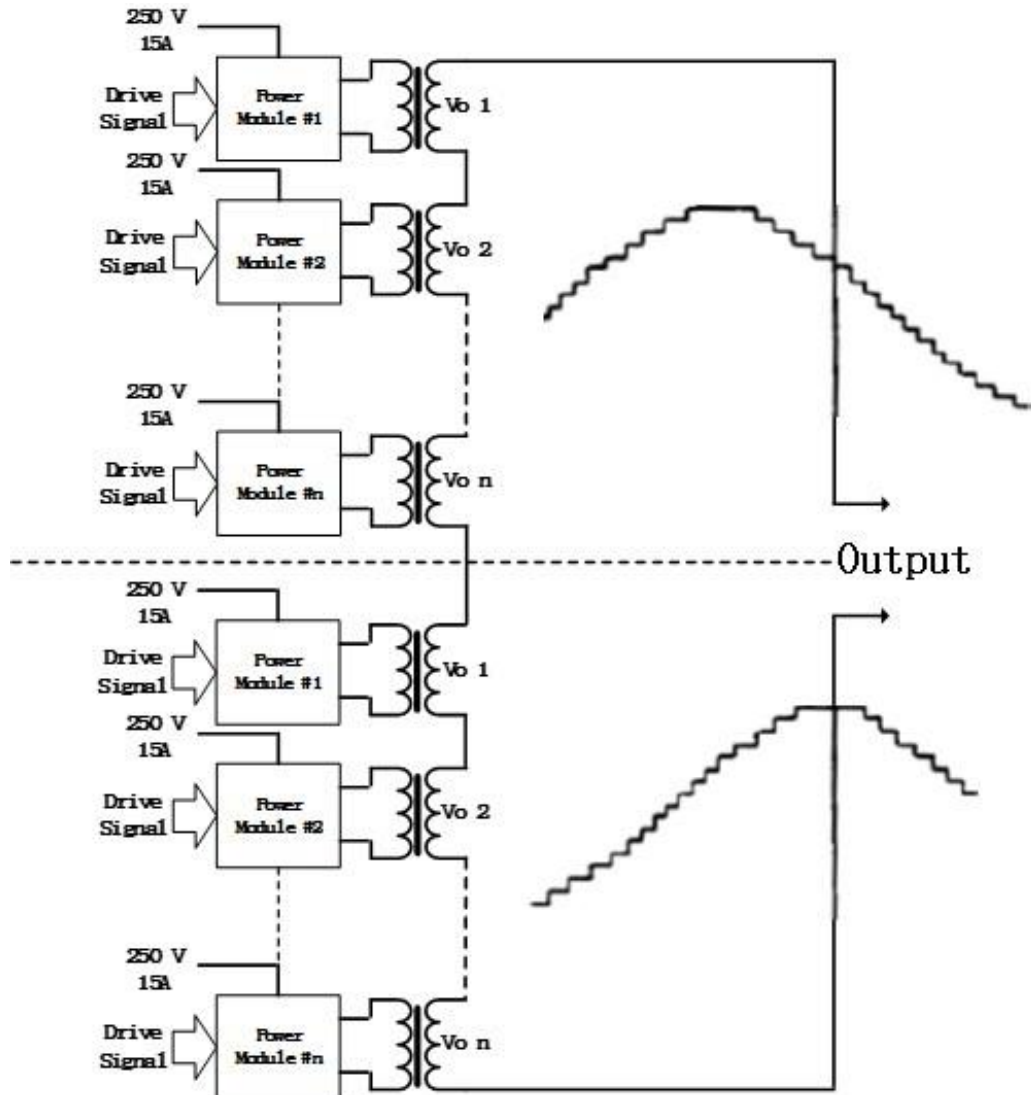


Fig.1. 4 Structure of Voltage Source Converter

Alternatively, the modular multilevel converter (MMC) is a newly introduced switch-mode converter topology with the potential HVDC transmission applications[8]. The structure and application is in Fig.1. 5. Usually, one AC side is connected to a power grid. MMC is very suitable for the case that two power grids are connected through DC transmission

line for electricity exchanging. Another application is to connect off shore wind farm, for transferring wind power to onshore grid[9]. In Europe, MMC is also used to offer power to traction intertie to provide a low frequency AC electrical energy[10].

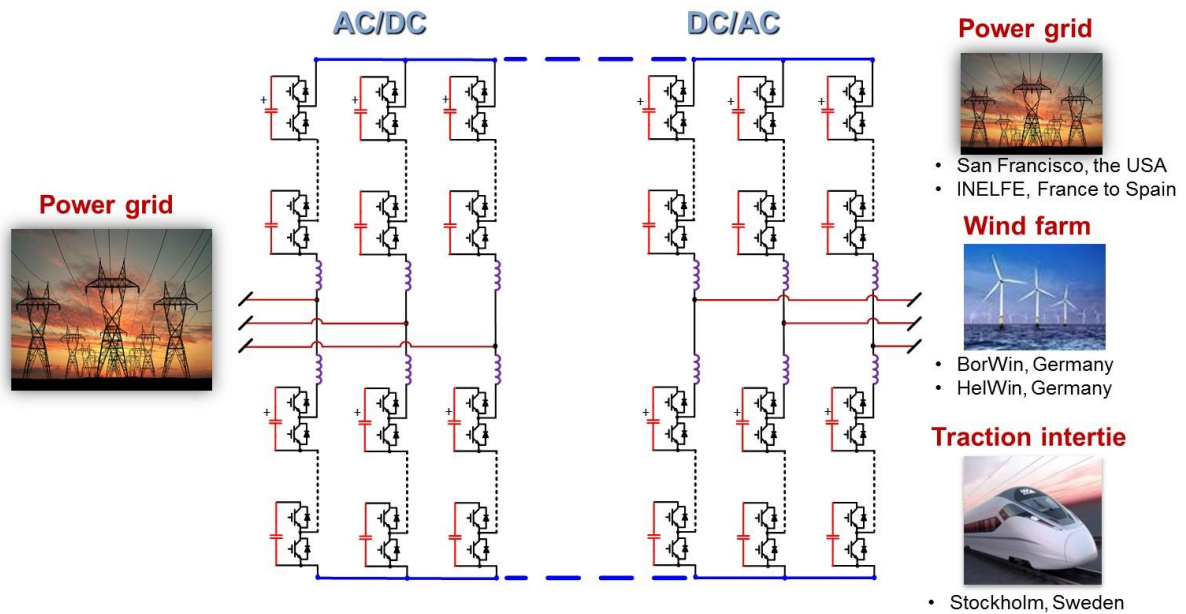


Fig.1. 5 Structure of MMC AC-DC combined system

### 1.2. Modular Multilevel Converter in HVDC

MMC is comprised of many sub-modules (SM) connected in series, in which each sub-module has a configuration of half-bridge or full-bridge converter[11]. MMC generates the line-frequency voltage waveform by switching each sub-module with low switching frequency and low harmonic level, which results in high efficiency[12][13][14]. As shown in Fig.1. 6 a 400MW/200kV MMC-based HVDC system was installed near San Francisco in the United States for the first time in the world[15].



Fig.1. 6 Trans Bay Cable in CA with MMC Technology

The modular multilevel converter (MMC) was first introduced in 2001[16]. This converter is an emerging cascaded multilevel converter with common dc bus, and considered suitable for VSC-HVDC transmission[17][18][19]. MMC is well scalable to high-voltage levels of power transmission based on cascade connection of multiple submodules (SMs) per arm, which also means a high number of output voltage levels (e.g., “Trans Bay Cable” Project is at 400 kV dc voltage, and about 200 SMs per arm [15]). The high number of voltage levels provides high-quality output voltage with low common-mode voltage, also known as zero-sequence voltage in a three-phase ac system[20]. Thus, only small or even no filters are required. Another advantage of the high-level number is

that low switching frequency modulation scheme can be adopted to reduce semiconductor switching losses[21][22].

The structure MMC is in Fig.1. 7. Compare with the previous version voltage source converter, the most significant difference is in MMC, the floating capacitors are used in sub-modules instead of isolated voltage sources. That means lots of bulky transformers are not needed at all.

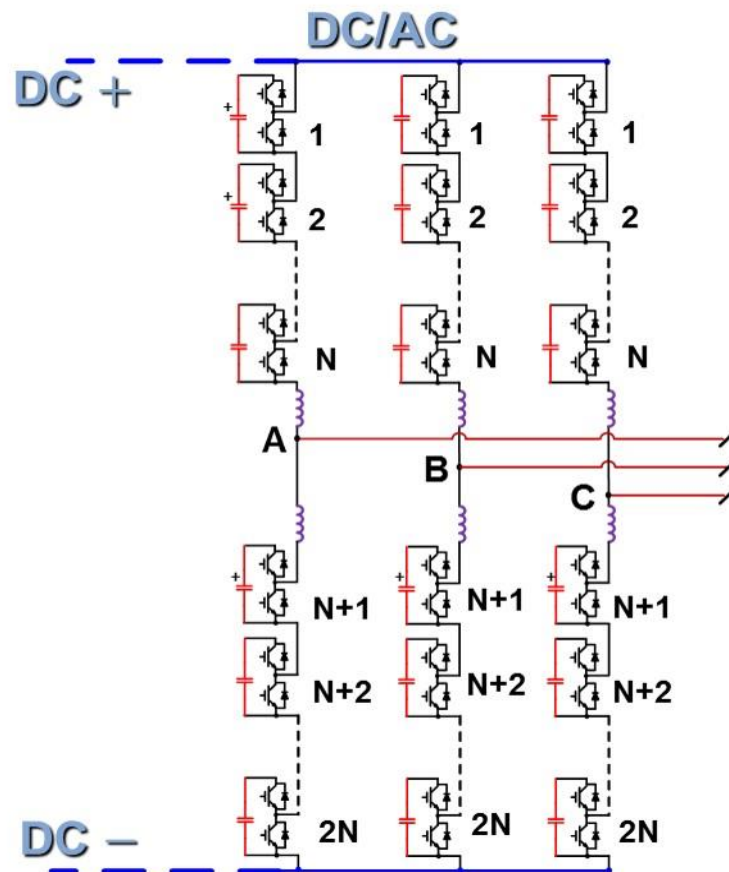


Fig.1. 7 Structure of Modular Multilevel Converter

In contrast to known VSCs (including the multilevel converters) the internal arm currents feature low  $di/dt$  and can be controlled, too. At first glance, when being compared to conventional VSC or multilevel VSC, the

---

new topology MMC offers several features, which are quite different and seem strange. Therefore, the main points are summarized in the following[23][24][25]:

The internal arm currents are not chopped; they are flowing continuously. The arm currents can be controlled by the converter control. Half the AC current is flowing in each arm.

Protection chokes can be inserted into the arms. They do not disturb operation or generate overvoltage for the semiconductors. The protection chokes limit the AC-current, whenever the DC-Bus is short circuited (fault condition).

The submodules are two terminal devices. There is no need to supply the DC-side-storage capacitor with energy no isolated, floating DC-supplies. This is true for real power or reactive power transmission of the converter in any direction or combination.

Voltage balancing (of the submodules) is not critical with respect to the timing of the pulses or the semiconductor switching times. It is assured by the converter control on a noncritical, larger time scale [23], [25].

The DC-link voltage of the converter can be controlled by the converter too (Fast control via the switching states). No DC-link capacitors

---

or filters are connected at the DC-Bus. The DC-Bus current and voltage are smooth and can be controlled by the converter, dynamically.

### ***1.3.Challenges of Modular Multilevel Converter***

Modular multilevel converters are being actively developed for offshore wind or tidal power collection and onwards transmission. Given the difficulties of constructing and maintaining an infrastructure in a hostile environment, it is important to keep the size as low as possible. In the current designs of an MMC submodule (SM) for 50 or 60 Hz ac grid-connected systems, the reservoir capacitor needs to absorb low order harmonics and hence accounts for over 50% of the total size and 80% of weight[26]. For most time, the energy buffering capability of the capacitor is not well utilized. The SM capacitor needs to be large enough (capacitance) to constrain the voltage ripple, while having sufficient ripple current capability to avoid overheating. Metalized polypropylene film (MPPF) capacitors are commonly used in MMC SMs due to their stability and ripple current capability. The sub-modules of Siemens is shown in Fig.1.8. In most industry products, the volume of the capacitors is more than 50% of the volume of the MMC. Hence, a method of reducing the circulating energy and capacitor voltage ripple has been widely pursued as an important research topic.



Fig.1. 8 Sub-module for MMC from Siemens

Controlling the circulating current offers opportunities for reducing the circulating energy. Winkelkemper, Korn, and Steimer proposed a method of injecting a second-order harmonic current to minimize the second-order voltage ripple of the capacitor [27]. By observing and analyzing the power of sub-modules, a proper harmonic current can be injected into the circuit with current control loop. This additional current can eliminate the second order power in the module and then eliminate the second order voltage in module capacitor. However, the benefits of this method are limited, since there is still a significant fundamental component in the capacitor voltage ripple.

---

The concept of injecting high-frequency voltage and circulating current was proposed in [28] to facilitate the start-up of induction motors with quadratic-torque loads. However, [28] only considers the dc and fundamental components in the arm current, and ignores the second-order component. Furthermore, the calculated circulating current is very complex and contains both low frequencies and high frequencies.

Recently, a novel concept of controlling the modulation was proposed to eliminate both the fundamental and second-order harmonic. The concept comes also from power analysis; the modulation index is related to the fundamental power in module. By setting a proper modulation index value, the fundamental power in module and fundamental voltage ripple in capacitor can be eliminated. In this method, full bridge module is required.

It should be noted that that even though there have been various methods proposed to reduce the capacitor voltage ripple, it was mostly done by trial and error. There is a lack of systematic approaches of addressing the means for capacitor ripple reduction. In general, the reported findings utilize the module power as a means to develop a control strategy. However, the minimum power flow needed from the source through the modules to the load is rather ambiguous.



---

A method of state trajectory analysis with the objective of delineating the needed power flow from the unwanted circulating energy is proposed in this thesis. The analysis method offers a graphical visualization of the effectiveness of the various proposed methods. Furthermore, it leads to a new proposed method that dramatically reduces the bulk of the circulating energy by eliminating both the fundamental and second-order harmonic components of power.

#### ***1.4.Thesis Outline***

Taking into account the challenges raised during the literature survey on the modular multilevel convertor, several issues have been addressed in this thesis:

In Chapter 1, Research background, application, motivation, challenges and opportunities are stated.

Due to the frequency flexibility and the cost saving for long distance transmission, the DC transmission line is more competitive in high voltage grid.

With the developing of semiconductor device, the new generation MOSFET and IGBT give one the opportunity to connect high voltage DC grid and AC grid by voltage source converters. Recently, the method of

---

using floating capacitor instead of the voltage source and bulky transformer was proposed, the modular multilevel convertor becomes most prominent interface converter used between DC and AC grid

The challenge of modular multilevel converter is that a large capacitance is required in order to suppress the voltage ripple. Therefore, reducing capacitor voltage attract lots of attention. However, there is a lack of systematic approaches of addressing the means for capacitor ripple reduction. This thesis also offers a graphical visualization of the effectiveness of the various proposed methods.

In Chapter 2, Basic working principle and structure of MMC is introduced

Pules width modulation and nearest level modulation are most popular modulation method for MMC. Moreover, PWM could suppress all low-order harmonics for multilevel converters and produce a sinusoidal output for MMC.

Average balance control and individual balance control are the basic control loop for MMC. With the basic control, the capacitor voltage of difference sub-modules is in the same level, which is the foundation of MMC basic operation and other control objects.

---

In order to analyze the working process clearly, MMC system can be simplified to one phase with only one module per arm. Basing on the PWM modulation and basic control, the complicated power flows in the MMC circuit is in-depth studied.

In Chapter 3, the State trajectory analysis is proposed. It enables one to gain a better understanding of the working principle of the MMC and offers a simple way to assess the effectiveness of the various control strategies with visual support.

Modulation index control method is proposed to reduce the fundamental voltage ripple and analyzed with state space analysis as the example 4

In Chapter 4, the concept is extended to the multi modules three phase system. And the loss evaluation offers one the trade of between semiconductor loss and voltage ripple reduction

The scaled down MMC hardware is introduced to verify the proposed concept and enlighten one new research opportunities.

Finally, summary and future work are provided

---

## Chapter 2 Basis Working Principle

### 2.1 Structure of MMC

Fig.2. 1 shows a three-phase MMC system with only a resistive load. The neutral point 'o' on the dc side is a fictitious point which divides the dc voltage to two equal parts of  $0.5V_{dc}$ . The converter topology consists of six phase arms. Each phase has an upper and a lower arm. There are n series-connected modules with an arm inductor in each arm. Each module has two switch devices and a capacitor in a half-bridge structure. In Fig.2. 1, the output is resistive and there is a neutral point 'm' of the three phases of the load. The n modules per arm can provide n+1 voltage levels.

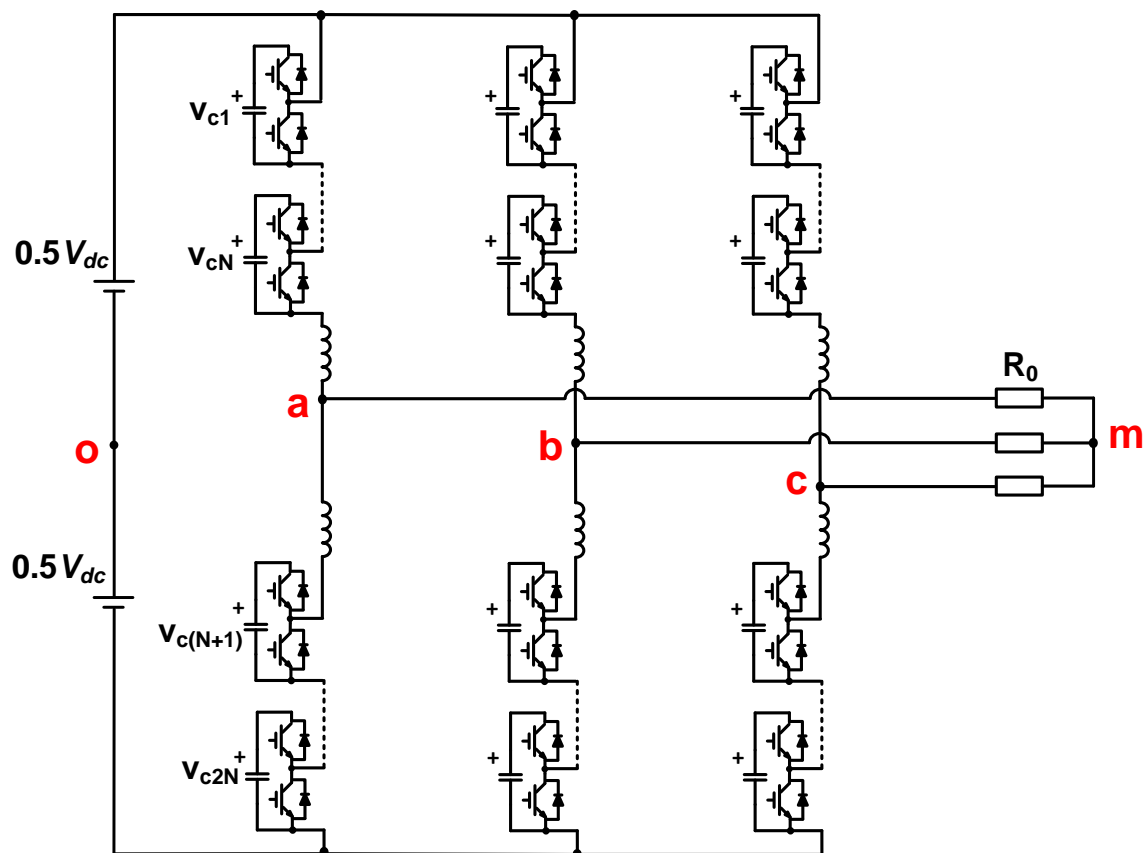


Fig.2. 1 Three phase MMC system

---

## ***2.2 Pulse Width Modulation for MMC***

The phase-shifted carrier-based PWM (PSC-PWM) method can naturally suppress all low-order harmonics for multilevel converters[29]. The details of the modified PSC-PWM method for one pair modules in upper and lower arm are shown in Fig.2. 2. The reference waveform for upper and lower arm is complementary. Comparing the carrier duty cycle waveform ( $v_{p\_ref}$ ,  $v_{n\_ref}$ ) with the triangle wave, the signal state condition of upper and lower module can be achieved. When half-bridge module is used, there are two switching states. The '1' state denotes when the upper switch is "on" and lower switch is "off;" the dc storage capacitor is connected in the phase. The '0' state denotes when the lower switch is "on" and the upper switch is "off." In the "0" state, the capacitor is bypassed from the phase arm. With the state condition of upper and lower module ( $S_1$  and  $S_2$ ), a sinusoidal output can be generated.

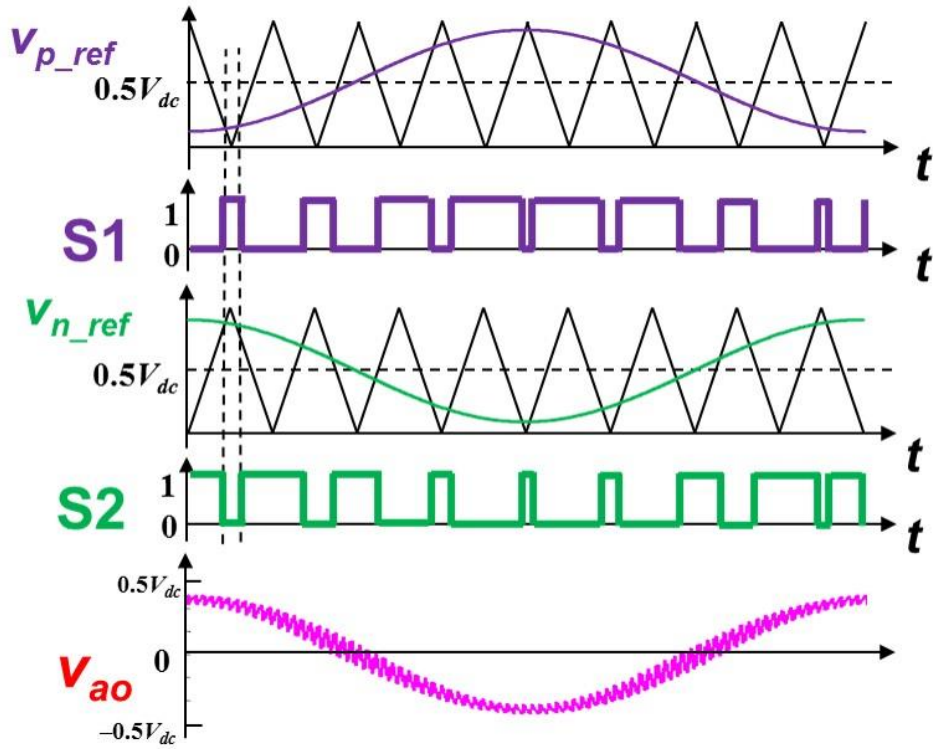


Fig.2. 2 PWM modulation for MMC with one module per arm

For an MMC with N number of SMs per arm, the reference arm voltages are compared with triangular carriers, each phase shifted by an angle of  $360 \text{ degrees}/N$ . As shown in Fig.2. 3. Compare with the same arm duty cycle wave, each module achieves their own switch state condition. Furthermore, in a N modules per arm MMC, the output voltage has N+1 level[ 30 ]. With 120 degrees' phase shift on reference wave, this modulation method can be extended to three phases system.

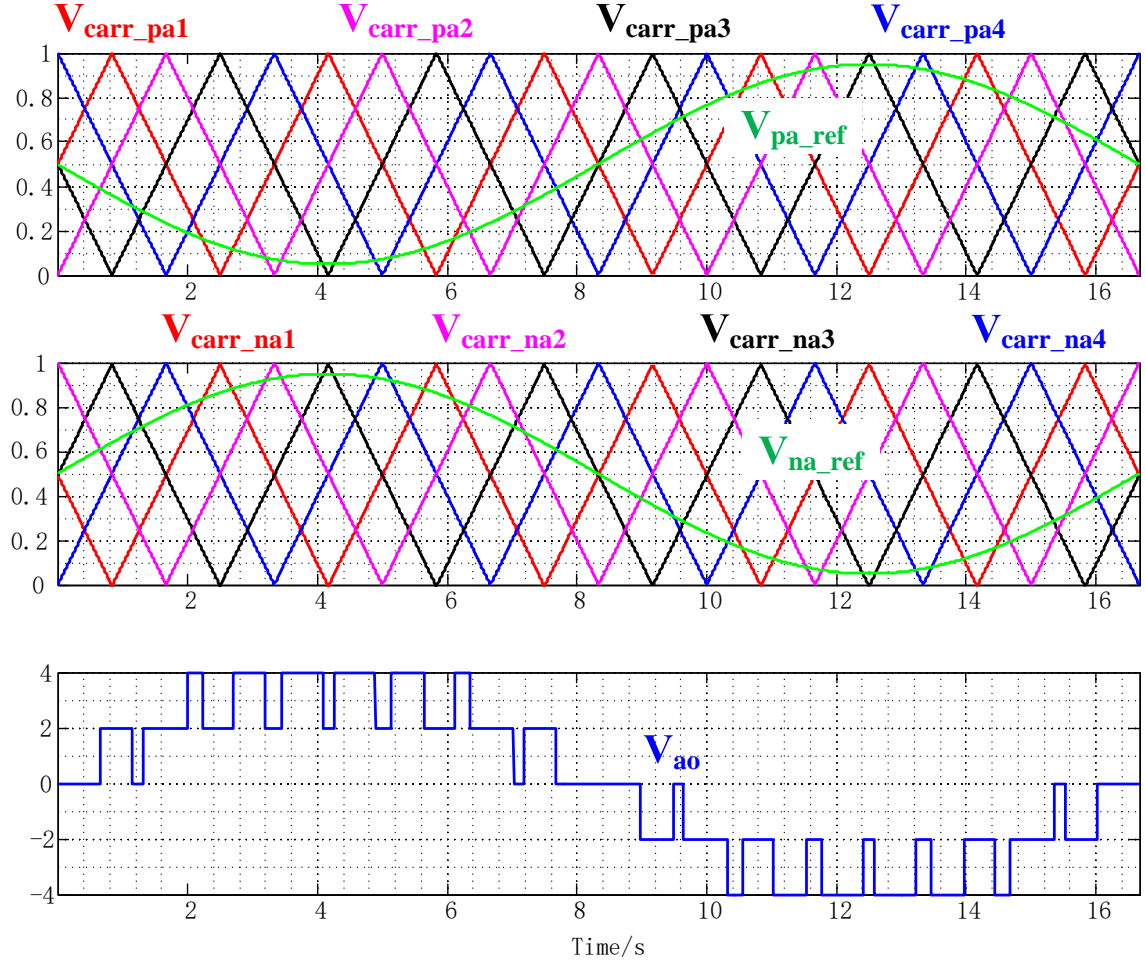


Fig.2. 3 PWM for multi modules per arm MMC

### 2.3 Nearest Level Modulation for MMC

Another effective modulation method is nearest level modulation[31][32]. Fig.2. 4 illustrates the working principle of the conventional NLM, with  $N$  module in one phase arm. The voltages are normalized by  $V_c$  to indicate the number of inserted SMs. The resulting output voltage  $v_a$  has a maximum level number of  $N + 1$ , with a step size of  $V_c$  and largest possible error of  $0.5v_c$ . The waveforms of the upper and lower arm step voltages  $V_{pa\_ref}$  and  $V_{na\_ref}$  are symmetrical to each other

with respect to the vertical  $y = N/2$  line (suppose the normalized voltage axis is the y-axis). Therefore, all the transition instants of  $V_{pa\_ref}$  and  $V_{na\_ref}$  are aligned.

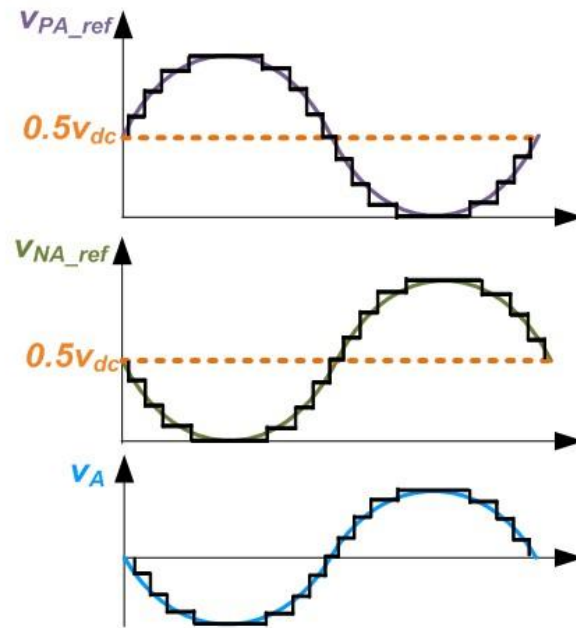


Fig.2. 4 working principle of the NLM

The control diagram of the conventional NLM method is illustrated in Fig.2. 5 The voltage reference is first normalized by the sub-module capacitor voltage  $v_c$ , then the round function gives the closest integer number of SMs to insert in order to approximate the voltage reference with the nearest voltage level. The nearest integer function or round function, is defined such that  $\text{round}(x)$  is the integer closest to  $x$ . The additional convention is that half-integers are always rounded to even number [33], for example  $\text{round}(1.5) = 2$ . The inserted upper and lower arm sub-module



numbers are:

$$n_{low} = \text{round}\left(\frac{N}{2} + \frac{NV_{A\_ref}}{V_{dc}}\right) \quad (2.1)$$

$$n_{up} = \text{round}\left(\frac{N}{2} - \frac{NV_{A\_ref}}{V_{dc}}\right) \quad (2.2)$$

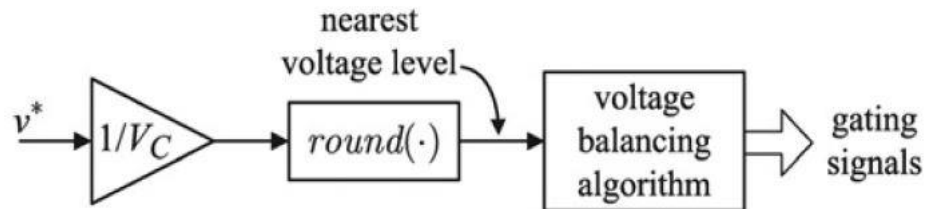


Fig.2. 5 The control diagram of NLM

The voltage balancing control is based on module voltage sorting. As shown in Fig.2. 6. , according to the sensed module voltage and arm current direction, N modules with highest voltage or lowest voltage are connected with phase arm. The inserted modules number N is based on the calculation in (2.1) and (2.2).

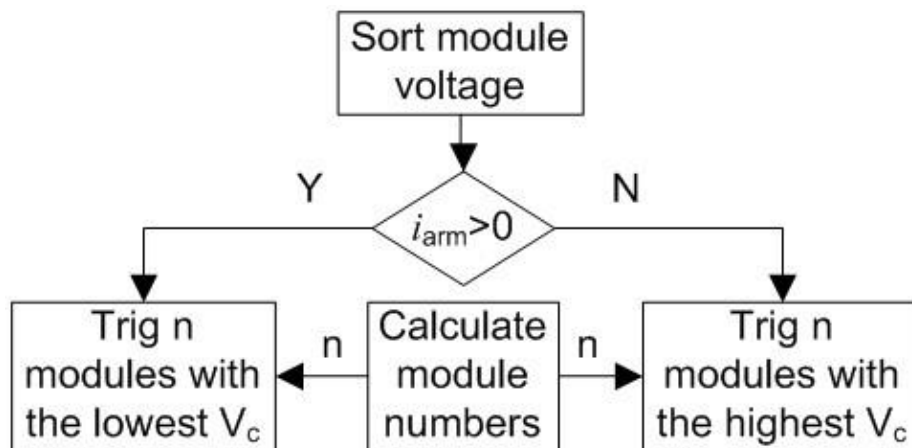


Fig.2. 6 The voltage balancing control of NLM

---

In the following simulation and analysis in this thesis, the pulse width modulation is used due to its flexibility and stability, especially for MMC with small module number.

#### **2.4 Basic control loop for voltage balancing in MMC**

Due to the large number of sub-modules and floating capacitors in modules, the voltage balancing of modules is an important issue. The first goal of voltage balancing is avoiding the over charge of the capacitor. Furthermore, balanced capacitor voltage is also an assumption for conventional modulation. Recent years, the solutions for this problem have been found and proposed in many literature such as [34][29].

The basic voltage-balancing control can be divided into:

- 1) Averaging control; and
- 2) Individual balancing control.

Averaging Control:

Fig.2. 7 shows a block diagram of the averaging control. It forces the one phase average voltage  $V_{c\_avr}$  to follow its command  $V_{c\_ref}$ , where  $V_{c\_avr}$  is given by

$$V_{c\_avr} = \frac{1}{N} \sum_{j=1}^N V_{c\_j} \quad (2.3)$$

Let a dc-loop current command of  $i_{Zref}$  be  $i_Z$ , as shown in Fig.2. 7.  $i_{Zref}$  is a result of a PI functioned comparison between  $V_{c\_avr}$  and  $V_{cref}$ .  $i_Z$  is the current which go through the upper and lower arm at the same time (so called “circulating current”).  $V_{ref\_avr}$  is the voltage command obtained from the averaging control.

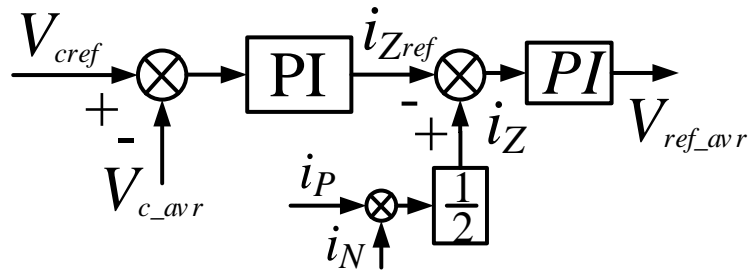


Fig.2. 7 control diagram for average balance control

When  $V_{cref} \geq V_{c\_avr}$ ,  $i_{Zref}$  increases. The function of the current minor loop forces the actual dc-loop current  $i_Z$  to follow its command  $i_{Zref}$ . As a result, this feedback control of  $i_Z$  enables  $V_{c\_avr}$  to follow its command  $V_{cref}$  without being affected by the load current  $i_o$ .

Individual balancing control.

The use of the balancing control described in [35] forces the individual capacitor voltage to follow its command  $V_{cref}$ . Fig.2. 8 shows a block diagram of the individual balancing control, where  $v_{ref\_Ij}$  is the voltage command obtained from the balancing control. It forms an active power between the voltage at the low voltage side of each sub-module,  $v_j$  and the corresponding arm current. Since the balancing control is based on either  $i_P$  or  $i_N$ , the polarity of  $v_{ref\_Ij}$  should be changed according to that of  $i_P$  or  $i_N$ .

When  $V_{cref} \geq v_j$  in the upper arm, a positive active power should be taken from the dc power supply into the upper sub-modules. When  $i_p$  is positive, the product of  $v_{ref\_Ij}$  and  $i_p$  forms the positive active power. When  $i_p$  is negative, the polarity of  $v_{ref\_Ij}$  should get inverse to take the positive active power.

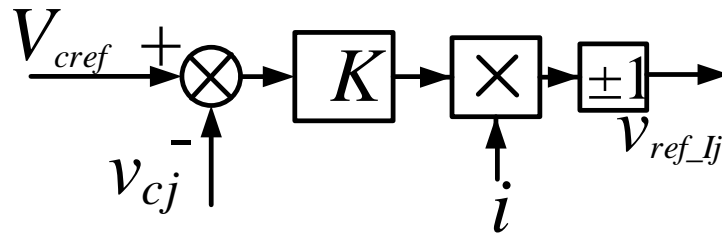


Fig.2. 8 control diagram of individual balance control

The final reference capacitor voltage is represented as

$$v_{ref}^* = v_{ref\_avr} + v_{ref\_Ij} + v_{ref} \quad (2.4)$$

where  $v_{c\_avr}$  comes from the average control loop,  $v_{ref\_Ij}$  is a result of individual balancing control. The  $v_{ref}$  is the original reference voltage. With the basic control method mentioned above, the fundamental function of MMC with multi sub-modules can be achieved.

## 2.5 Simplification of MMC

Base on the carrier phase shifted pulse width modulation mentioned previous, the basic average voltage control and individual balance control, a simulation of 3 phase MMC with 4 modules per arm as in Fig.2. 1 is proposed. The parameters of the simulation are in Table 2. 1.

Table 2. 1 SIMULATION PARAMETERS

DC source voltage	4800 V
Line frequency	60 Hz
Arm inductance	4 mH
Modulation Index	0.8
SM capacitance	750 $\mu$ F
Switching frequency	5 kHz
Load Resistor	3.2 Ohms
Number of Module	4 per arm

Fig.2. 9 shows the results of two of three phase for the simulation above. The output currents of phase A and phase B,  $i_a$  and  $i_b$ , are stranded sinusoidal wave, meaning the object of the MMC system can be achieved by using the conventional PWM. Meanwhile, the module capacitor voltages  $v_{ca_{1-8}}$ ,  $v_{cb_{1-8}}$  are well balanced by the basic control. Due to the symmetric of three phase and also from the simulation results in Fig.2. 99, we could also notice that the performances of arm currents  $i_{pa}$ ,  $i_{pb}$  and  $i_{na}$ ,  $i_{nb}$  are very similar, so are the module capacitor voltage. The only difference is the phase shift. Therefore, in analysis aspect, we could focus

on only one phase instead of three phases. In the following discuss in this thesis, the analyses are mainly based on one phase system.

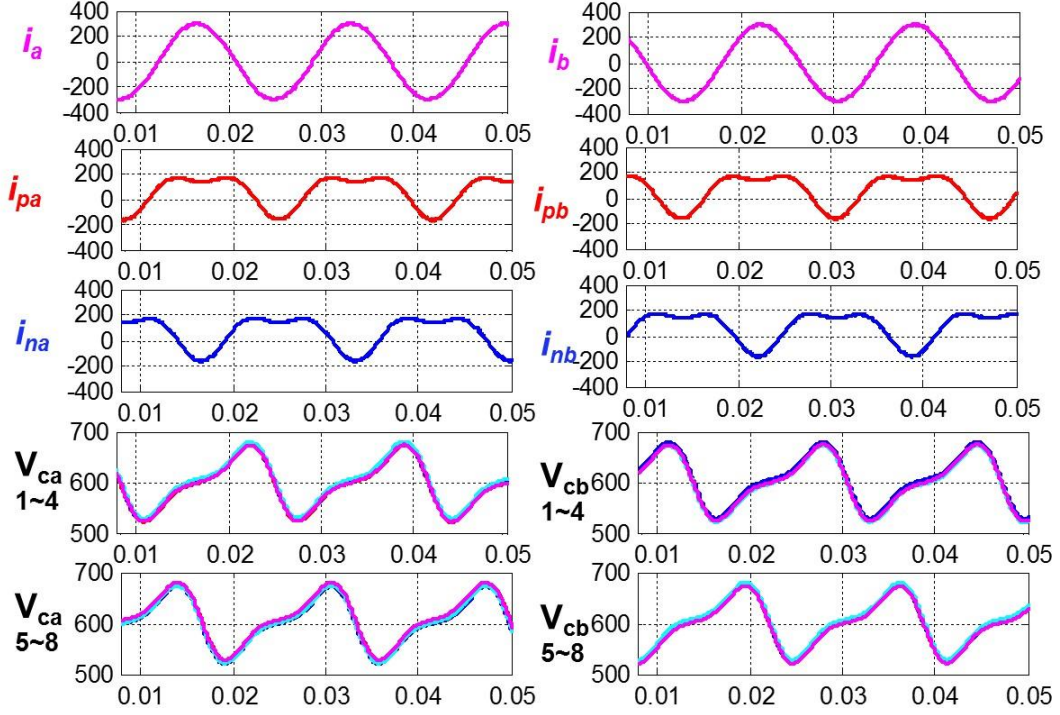


Fig.2. 9 Simulation results of three phase MMC

$$\begin{bmatrix} \frac{di_1}{dt} \\ \frac{dv_{c1}}{dt} \\ \vdots \\ \frac{dv_{cN}}{dt} \\ \frac{di_2}{dt} \\ \frac{dv_{c(N+1)}}{dt} \\ \vdots \\ \frac{dv_{c2N}}{dt} \end{bmatrix} = \begin{bmatrix} -\frac{R_0}{L} & -\frac{d_1}{L} & \dots & -\frac{d_N}{L} & \frac{R_0}{L} & 0 & \dots & 0 \\ \frac{d_1}{C} & 0 & \dots & 0 & 0 & 0 & \dots & 0 \\ \vdots & 0 & \dots & 0 & 0 & 0 & \dots & 0 \\ \frac{d_N}{C} & 0 & \dots & 0 & 0 & 0 & \dots & 0 \\ \frac{R_0}{L} & 0 & \dots & 0 & -\frac{R_0}{L} & -\frac{d_{N+1}}{L} & \dots & -\frac{d_{2N}}{L} \\ 0 & 0 & \dots & 0 & \frac{d_{N+1}}{C} & 0 & \dots & 0 \\ \vdots & 0 & \dots & 0 & \vdots & 0 & \dots & 0 \\ 0 & 0 & \dots & 0 & \frac{d_{2N}}{C} & 0 & \dots & 0 \end{bmatrix} \begin{bmatrix} i_1 \\ v_{c1} \\ \vdots \\ v_{cN} \\ i_2 \\ v_{c(N+1)} \\ \vdots \\ v_{c2N} \end{bmatrix} + \begin{bmatrix} \frac{V_{dc}}{2L} \\ 0 \\ \vdots \\ 0 \\ \frac{V_{dc}}{2L} \\ 0 \\ \vdots \\ 0 \end{bmatrix} \quad (2.5)$$

The matrix above is the differential equations of a single-phase MMC with N sub-modules in phase. In terms of the matrix, the upper arm and lower arm equation are coupled by the term in the red box, which contains only the components of load.

$$i_o = v_o / R_0 \quad (2.6)$$

Equation (2.6) is the expression of the output current. Substituting (2.6) into matrix (2.5), a decoupled matrix can be achieved, as follows below.

$$\begin{aligned}
 & \begin{bmatrix} \frac{di_1}{dt} \\ \frac{dv_{c1}}{dt} \\ \vdots \\ \frac{dv_{cN}}{dt} \end{bmatrix} = \begin{bmatrix} 0 & -\frac{d_1}{L} & \dots & -\frac{d_N}{L} & 0 & 0 & \dots & 0 \\ \frac{d_1}{C} & 0 & \dots & 0 & 0 & 0 & \dots & 0 \\ \vdots & 0 & \dots & 0 & 0 & 0 & \dots & 0 \\ \frac{d_N}{C} & 0 & \dots & 0 & 0 & 0 & \dots & 0 \end{bmatrix} \begin{bmatrix} i_1 \\ v_{c1} \\ \vdots \\ v_{cN} \end{bmatrix} + \begin{bmatrix} \frac{V_{dc}}{2L} - \frac{v_{ao}}{L} \\ 0 \\ \vdots \\ 0 \end{bmatrix} \\
 & \begin{bmatrix} \frac{di_2}{dt} \\ \frac{dv_{c(N+1)}}{dt} \\ \vdots \\ \frac{dv_{c2N}}{dt} \end{bmatrix} = \begin{bmatrix} 0 & 0 & \dots & 0 & 0 & -\frac{d_{N+1}}{L} & \dots & -\frac{d_{2N}}{L} \\ 0 & 0 & \dots & 0 & \frac{d_{N+1}}{C} & 0 & \dots & 0 \\ \vdots & 0 & \dots & 0 & \vdots & 0 & \dots & 0 \\ 0 & 0 & \dots & 0 & \frac{d_{2N}}{C} & 0 & \dots & 0 \end{bmatrix} \begin{bmatrix} i_2 \\ v_{c(N+1)} \\ \vdots \\ v_{c2N} \end{bmatrix} + \begin{bmatrix} \frac{V_{dc}}{2L} + \frac{v_{ao}}{L} \\ 0 \\ \vdots \\ 0 \end{bmatrix} \quad (2.7)
 \end{aligned}$$

In (2.7), with considering the load components as given value and moving them into the constant matrix, all the terms in the red boxes are zero, meaning that the matrix can be seen as two decoupled parts. The

upper part of the equation represents the upper arm information of the circuit, and the lower part of the equation stands for the lower arm.

$$\begin{bmatrix} \frac{di_1}{dt} \\ \frac{dv_{c1}}{dt} \\ \vdots \\ \frac{dv_{cN}}{dt} \end{bmatrix} = \begin{bmatrix} 0 & -\frac{d_1}{L} & \dots & -\frac{d_N}{L} \\ \frac{d_1}{C} & 0 & \dots & 0 \\ \vdots & 0 & \dots & 0 \\ \frac{d_N}{C} & 0 & \dots & 0 \end{bmatrix} \begin{bmatrix} i_1 \\ v_{c1} \\ \vdots \\ v_{cN} \end{bmatrix} + \begin{bmatrix} \frac{V_{dc}}{2L} - \frac{v_{ao}}{L} \\ 0 \\ \vdots \\ 0 \end{bmatrix} \quad (2.8)$$

Matrix (2.8) is the upper part of (2.7), which contains the upper arm information. If all the duty cycles  $d$  are assumed as same value and all capacitor voltages  $v_c$  are well balanced, the information in this complex system can be represented by a 2X2 matrix in the red box.

Basing on the decoupling concept above, the multi module circuit can be represented by the simplified circuit with only one module per arm, showing in Fig.2. 10 . The differential equations of the simplified circuit are represented as:

$$\begin{bmatrix} \frac{di_1}{dt} \\ \frac{dv_{c1}}{dt} \end{bmatrix} = \begin{bmatrix} 0 & -\frac{d_1}{L} \\ \frac{d_1}{C} & 0 \end{bmatrix} \begin{bmatrix} i_1 \\ v_{c1} \end{bmatrix} + \begin{bmatrix} \frac{V_{dc}}{2L} - \frac{v_o}{L} \\ 0 \end{bmatrix} \quad (2.9)$$



$$\begin{bmatrix} \frac{di_2}{dt} \\ \frac{dv_{c2}}{dt} \end{bmatrix} = \begin{bmatrix} 0 & -\frac{d_2}{L} \\ \frac{d_1}{C} & 0 \end{bmatrix} \begin{bmatrix} i_1 \\ v_{c2} \end{bmatrix} + \begin{bmatrix} \frac{V_{dc}}{2L} + \frac{v_o}{L} \\ 0 \end{bmatrix} \quad (2.10)$$

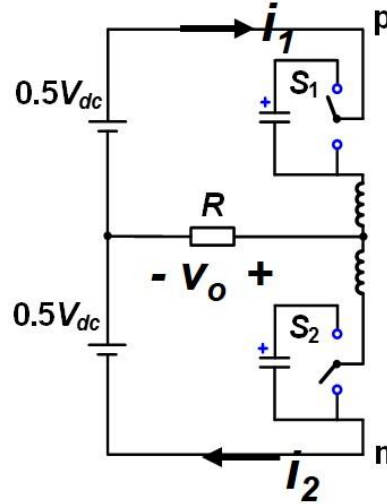


Fig.2. 10 Simplified one phase MMC circuit with one module per arm

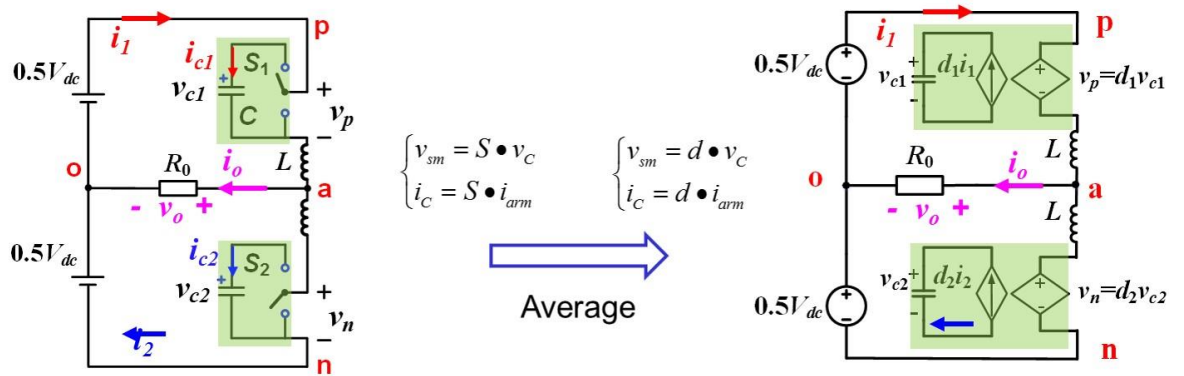


Fig.2. 11 Replacing switching model with average model in MMC

Our analysis in this thesis is focused on the line frequency problems, the switching frequency performance of the circuit is not our concern. Therefore, as in Fig.2. 11 the switching model can be replaced with the average model with the following equations:

$$\begin{cases} v_{sm} = S \bullet v_C \\ i_C = S \bullet i_{arm} \end{cases} \quad (2.11)$$

$$\begin{cases} v_p = d \bullet v_C \\ i_C = d \bullet i_{arm} \end{cases} \quad (2.12)$$

### 2.1 Analysis of simplified MMC circuit

Fig.2. 12 is the simplified one module circuit with average model. The ac reference output voltage and current can be defined as:

$$v_o = 0.5V_{dc}M \cos(\omega t) \quad (2.12)$$

$$i_o = 0.5V_{dc}M \cos(\omega t) / R \quad (2.13)$$

where M is the modulation index.

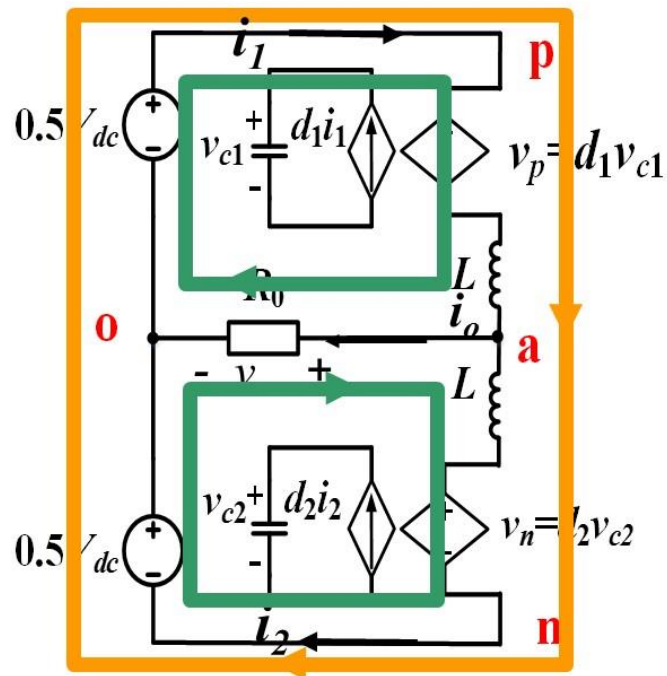


Fig.2. 12 The average circuit model with current loop

---

In the conventional open-loop control law of the MMC, the duty cycle of the upper module  $d_1$  and lower module  $d_2$  is set based on Kirchhoff's voltage law (KVL).

$$\begin{cases} 0.5V_{dc} = d_1 v_{c1} + v_o + v_L \\ 0.5V_{dc} = d_2 v_{c2} - v_o + v_L \end{cases} \quad (2.14)$$

where  $v_{c1}$  and  $v_{c2}$  are the sub-module capacitor voltages. For the purpose of defining a simple modulation control law, one can first assume that the voltage ripples of the sub-module capacitor voltage are negligible. Hence  $v_{c1}$  and  $v_{c2}$  are replaced by  $V_{dc}$ . Furthermore, because the arm inductor is a relatively small value, the voltage on the inductor can also be neglected. Thus the expression of duty cycle can be written as

$$\begin{cases} d_1 = 0.5 - 0.5M \cos \omega t \\ d_2 = 0.5 + 0.5M \cos \omega t \end{cases} \quad (2.15)$$

In the circuit in **Error! Reference source not found.**, due to the KCL, the currents have the following relationship.

$$i_o = i_1 - i_2 \quad (2.16)$$

$$i_1 = I_{dc} + i_{har} + 0.5i_o \quad (2.17)$$

$$i_2 = I_{dc} + i_{har} - 0.5i_o \quad (2.18)$$

where the upper arm current is  $i_1$ , the lower arm current is  $i_2$  and output

---

current is  $i_o$ . From (2.17) and (2.18), we know that the arm currents  $i_1$  and  $i_2$  have three components. One of the components is from half the output current  $i_o$ , the green loop in Fig.2. 12. The other two components are the currents which do not go to the output, but go through from the upper arm to the lower arm and circulate in the circuit. In the Fig.2. 12, the circulating current is in orange color. Variable  $i_{har}$  represents the low-frequency harmonics. Since  $i_{har}$  does not flow into the load,  $i_{har}$  offers a free variable to control.

With the simple duty cycle control law in (2.15), a simulation of the circuit in Fig.2. 12 was made to observe the base performance of this simplest case with the simulation parameters in Table 2. 2.

Table 2. 2 SIMULATION PARAMETERS

DC source voltage	600 V
Line frequency	60 Hz
Arm inductance	2 mH
Modulation Index	0.8
SM capacitance	750 $\mu$ F
Switching frequency	5 kHz
Load Resistor	3.2 Ohms

The simulation results are shown in Fig.2. 13. The output voltage is a

sinusoidal wave with 240V peak voltage. That means even with the simple control law in (2.15), the target output goal can be achieved. In the arm current, there are three components, which were defined in (2.17) and (2.18). As shown by the results, the harmonic current  $i_{har}$  is a second-order harmonic, and the dc bias of arm current  $I_{dc}$  is about 15A.

It is clear that there are significant ripples in the sub-module capacitor voltage. The peak-to-peak value of the voltage ripple is around 127V. By observing the spectrum, we can see that the fundamental voltage also contributes voltage ripple. Meanwhile, the second-order voltage ripple is also very obvious. This means a large capacitor bank and high cost are required. Several control strategies proposed previously, aimed at reducing the capacitor size, are analyzed in the following sections.

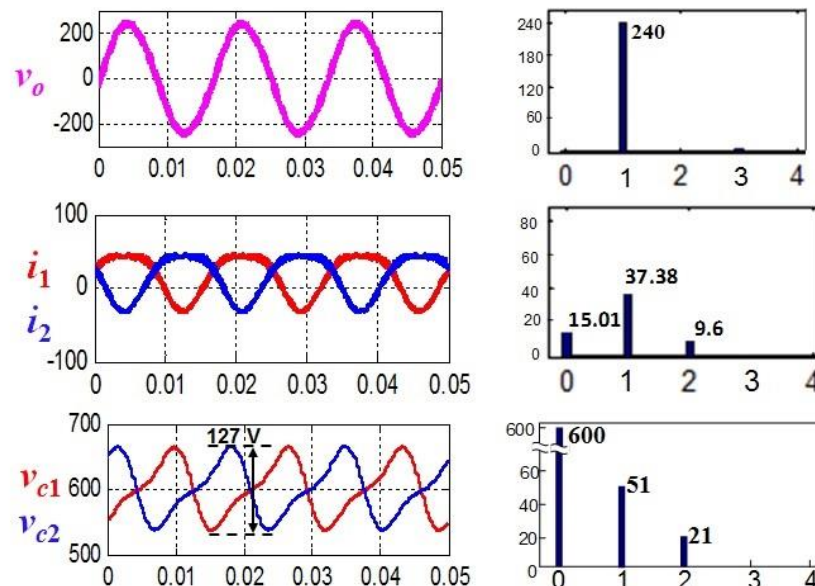


Fig.2. 13 Simulation results for simple control law

---

In [16], the reason for the capacitor voltage ripple is explained. The module plays a significant role for power transfer in this circuit. As explained in [16], the module must produce a power offering to load or transfer with the source and even other modules. The produced power has harmonics. However, the only component which can carry that harmonic power is the capacitor. The inductor voltage and inductor power, which are very small, will be assumed to be negligible. In order to analyze this issue clearly, a power flow analysis is necessary. In following power analysis, the inductor voltage and inductor power are ignored.

$$p_p = i_1 v_{pa} \quad (2.19)$$

$$p_n = i_2 v_{an} \quad (2.20)$$

where  $p_p$  is the upper module power and  $p_n$  is the lower module power, and  $i_1$  and  $i_2$  are the arm current,  $v_{pa}$  is the upper arm voltage from point p to point a, and  $v_{an}$  is the lower arm voltage. Using the KVL, the expression of  $v_{pa}$  and  $v_{an}$  can be derived:

$$v_{pa} = 0.5V_{dc} - V_o \cos \omega t \quad (2.21)$$

$$v_{an} = 0.5V_{dc} + V_o \cos \omega t \quad (2.22)$$

Substituting (2.17) and (2.21) into (2.19) and substituting (2.18) and (2.22) into (2.20), the expression of the arm power can be calculated:

$$p_p = \left(\frac{1}{2}I_o V_{dc} - I_{dc} V_o + \frac{1}{2}I_h V_o\right) \cos \omega t - \frac{1}{4}V_o I_o \cos 2\omega t + \frac{1}{2}i_{har} V_{dc} + \frac{1}{2}I_h V_o \cos 3\omega t \quad (2.23)$$

$$p_n = -\left(\frac{1}{2}I_o V_{dc} - I_{dc} V_o + \frac{1}{2}I_h V_o\right) \cos \omega t - \frac{1}{4}V_o I_o \cos 2\omega t + \frac{1}{2}i_{har} V_{dc} - \frac{1}{2}I_h V_o \cos 3\omega t \quad (2.24)$$

In (2.25), it describes the relationship of the upper module power and arm current. The components in (2.25) in orange color are associated with the orange part in (2.17), which are “circulating current”. The components in (2.25) in green color are associated with the green part in (2.17) which are load current. Based on the common understanding of circulating current, the circulating current produces the circulating power. However, the question is: In this circuit, is all the circulating power produced by circulating current? In order to answer this question, power flow analysis is required.

$$\begin{aligned}
 p_p = i_1 v_{pa} = & \frac{1}{4} I_o V_o - \frac{1}{4} I_o V_o + \left( \frac{1}{2} I_o V_{dc} - I_{dc} V_o + \frac{1}{2} I_h V_o \right) \cos \omega t \\
 & - \left( \frac{1}{4} I_o V_o - I_h V_{dc} \right) \cos 2\omega t + \frac{1}{2} I_h V_o \cos 3\omega t
 \end{aligned} \tag{2.25}$$

To understand the function and relationship of power flows, the load power and total source power also need to be observed.

$$p_o = \frac{1}{2} I_o V_o + \frac{1}{2} I_o V_o \cos 2\omega t \tag{2.26}$$

$$p_s = \frac{1}{2} V_{dc} (i_1 + i_2) = \frac{1}{2} I_o V_o + i_{har} V_{dc} \tag{2.27}$$

where  $p_o$  is the load power which has a dc term and an ac term, and  $p_s$  is the total source power, which also has a dc term and an ac term.

By observing the equations above, we can summarize several relationships.

- 
- a) The dc term in  $p_o$  equals the dc terms in  $p_s$ ;
  - b) The second-order harmonic ac term in the load power equals twice the second-order harmonic term in the upper and lower arm power;
  - c) The ac power in the source, which relates to  $i_{har}$ , equals to the harmonic term in the arm power;
  - d) In the upper arm power and lower arm power equations, the fundamental and third-order harmonic components have opposite signs.

Even though the power transfer process in this circuit is very complicated, we can derive the following observations:

- a) The dc power in the load comes from the source;
- b) The phase arm contributes second-order power to the load;
- c) The phase arm receives power from the source;
- d) The AC power switches between the upper arm and lower arm.

The power flow analysis above can be shown in Fig.2. 14. Moreover, the relationship of arm current and module power is summarized in Table 2. 3. By observing the table, we could notice that the circulating harmonic power is associated with all the components of arm current, not only the so



called “circulating current”.

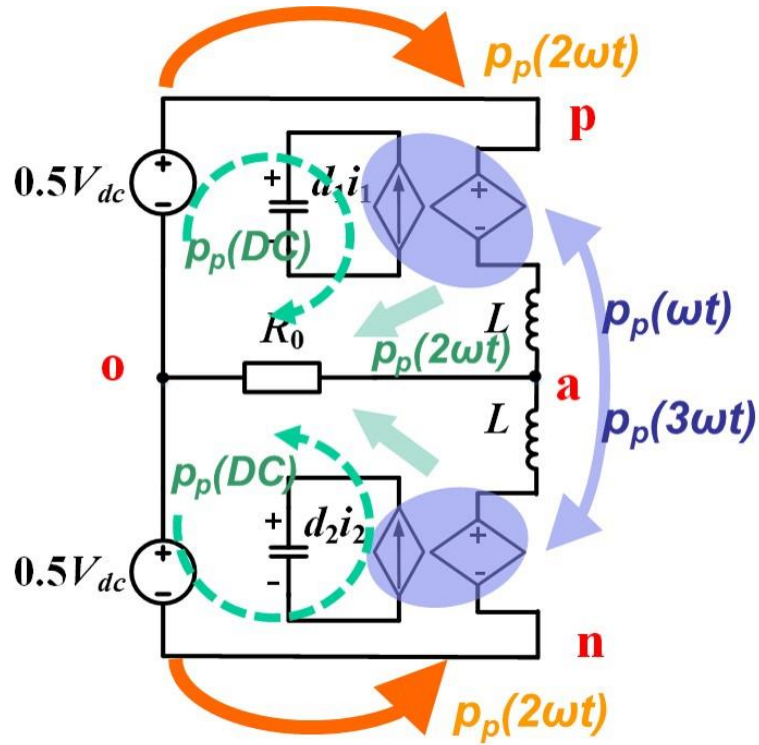


Fig.2. 14. Power transfer diagram

Table 2. 3 SUMMARY OF ARM CURRENT AND MODULE POWER

$i_1 \backslash p_p$	$p_p(DC)$	$p_p(\omega t)$	$p_p(2\omega t)$	$p_p(3\omega t)$
$I_{dc}$	$\frac{1}{4} I_o V_o$	$-I_{dc} V_o$		
$\frac{1}{2} I_o \cos \omega t$	$-\frac{1}{4} I_o V_o$	$\frac{1}{2} I_o V_{dc}$	$-\frac{1}{4} I_o V_o$	
$I_h \cos 2\omega t$		$\frac{1}{2} I_h V_o$	$\frac{1}{2} I_h V_{dc}$	$\frac{1}{2} I_h V_o$

Using Fig.2. 14 and Table 2. 3 , the function of the modules can be

---

explained in terms of energy storage and transfer. It can be noted that the module has a significant role in the power flow process for this circuit. However, the amount of energy storage and transfer that is essential for the intended purpose is still unknown. In the sections below, the state trajectory analysis is employed to help minimize the circulating power and thus minimize the voltage ripple.

---

## Chapter 3 State Space Analysis

### *3.1 Introduction of State Space Analysis*

In the previous section, Fig.2. 13 shows that the arm current and capacitor voltage are the state variables in each module. Hence the four state variables for the MMC are defined as  $i_1$ ,  $i_2$ ,  $v_{c1}$ , and  $v_{c2}$ . Because  $i_1$  and  $i_2$  are related by (3.1), they are not independent. Therefore, there are only three independent variables. Thus, one can use a 3D state trajectory, with the three variables  $i_1$ ,  $v_{c1}$ , and  $v_{c2}$  to represent the system.

$$i_1 - i_2 = i_o \quad (3.1)$$

Fig.3. 1 illustrates the 3D state trajectories. To facilitate visual support, the 3D state trajectory is projected into three 2-D planes, as shown in Fig.3.

2.

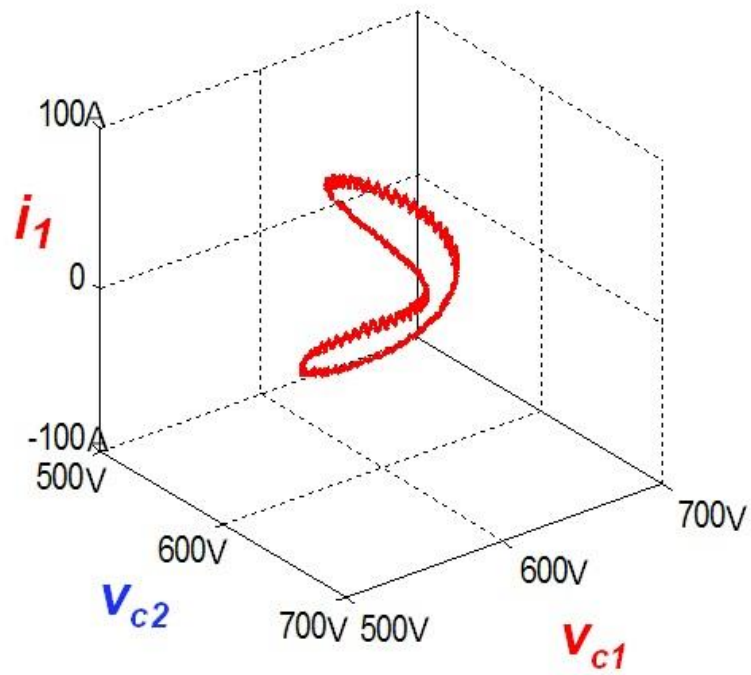


Fig.3. 1 3D state space diagram for MMC

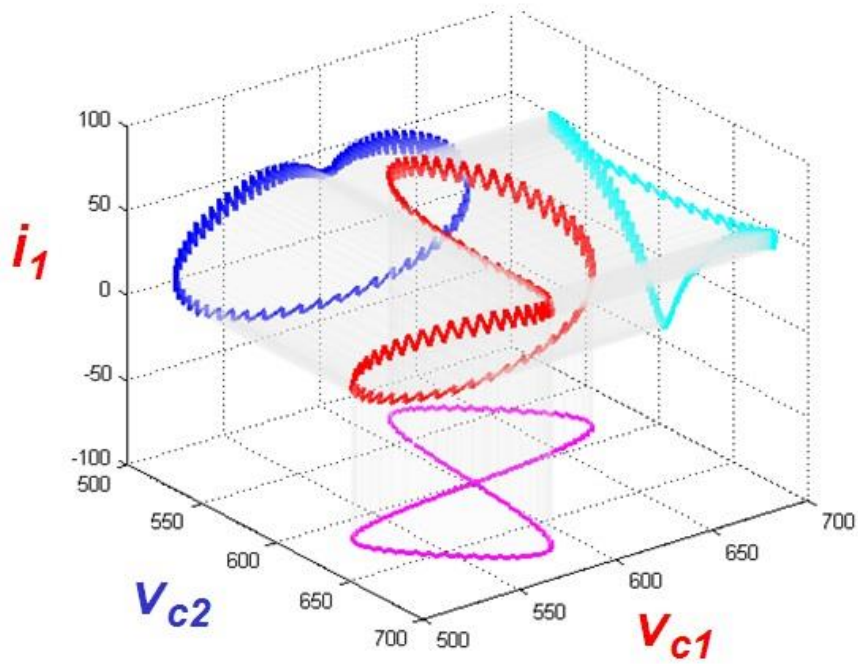


Fig.3. 2 2D state plane projection for MMC

The capacitor voltage of upper and lower module can be calculated using (6) and (7).

---


$$\begin{aligned}
v_{c1} &= V_{dc} + \frac{1}{C} \int d_1 i_1 dt \\
&= \frac{1}{C} \frac{1}{\omega} \left( \frac{2V_{dc}}{V_o} - \frac{V_o}{4V_{dc}} \right) I_{dc} \sin \omega t - \frac{MI_h}{4C\omega} \sin \omega t - \frac{1}{C} \frac{I_{dc}}{4\omega} \sin 2\omega t + \frac{1}{C} \frac{I_h}{4\omega} \sin 2\omega t - \frac{V_o I_h}{24V_{dc} C \omega} \sin 3\omega t
\end{aligned} \tag{3.2}$$

$$\begin{aligned}
v_{c2} &= V_{dc} + \frac{1}{C} \int d_2 i_2 dt \\
&= -\frac{1}{C} \frac{1}{\omega} \left( \frac{2V_{dc}}{V_o} - \frac{V_o}{4V_{dc}} \right) I_{dc} \sin \omega t - \frac{MI_h}{4C\omega} \sin \omega t - \frac{1}{C} \frac{I_{dc}}{4\omega} \sin 2\omega t + \frac{1}{C} \frac{I_h}{4\omega} \sin 2\omega t + \frac{V_o I_h}{24V_{dc} C \omega} \sin 3\omega t
\end{aligned} \tag{3.3}$$

In the capacitor voltage, there are DC components, which is the DC voltage bias, fundamental, second order and third order harmonics. Since the capacitor is the only energy storage device within the module, the capacitor voltage equation is very similar to the module power equation.

The state trajectory in Fig.3. 3 shows the relationship between  $i_l$  and  $v_{c1}$ , the second-order harmonic in the arm current with clear visual support.

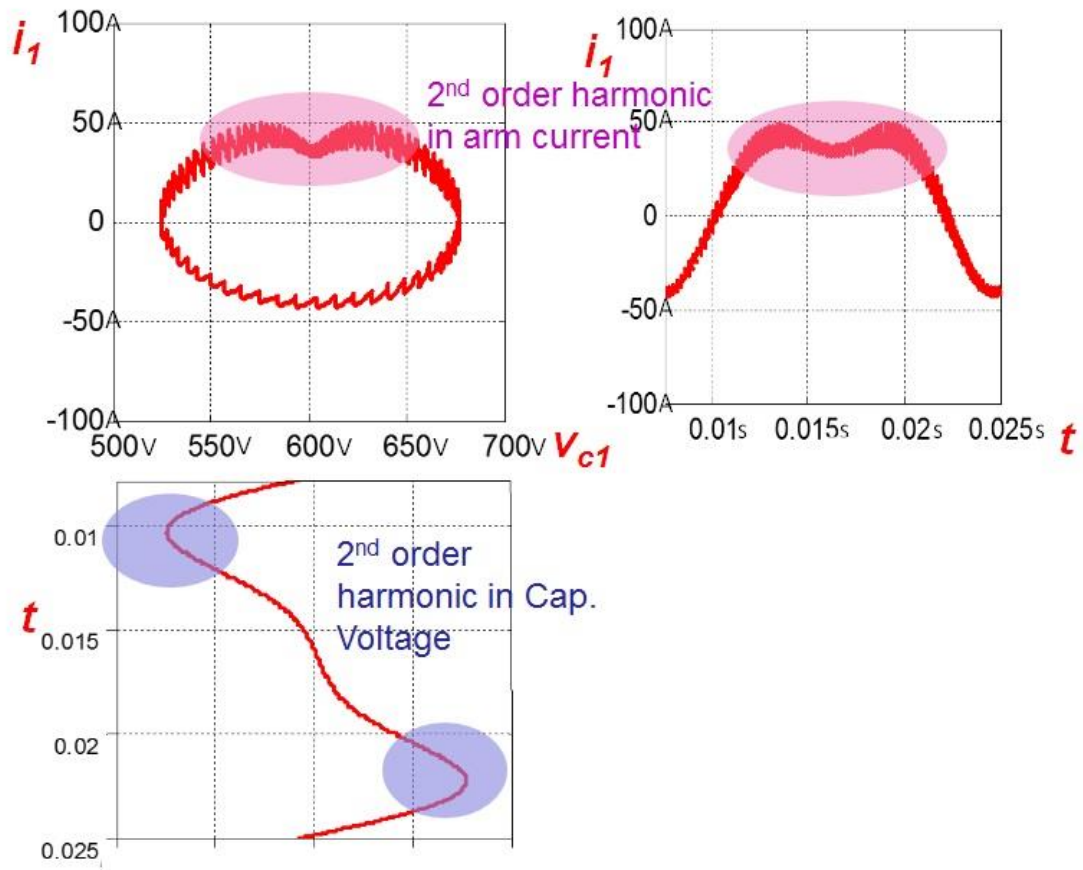


Fig.3. 3 The state plane trajectory of upper arm current and module voltage

The size of the state trajectory in one cycle of operation is proportional to its energy; i.e., a larger loop leads to a higher energy content. For example, illustrates that the loop size decreases with a larger load resistor.

Fig.3. 4 shows the state trajectory of  $i_1$  and  $v_{c1}$  with different power ratings

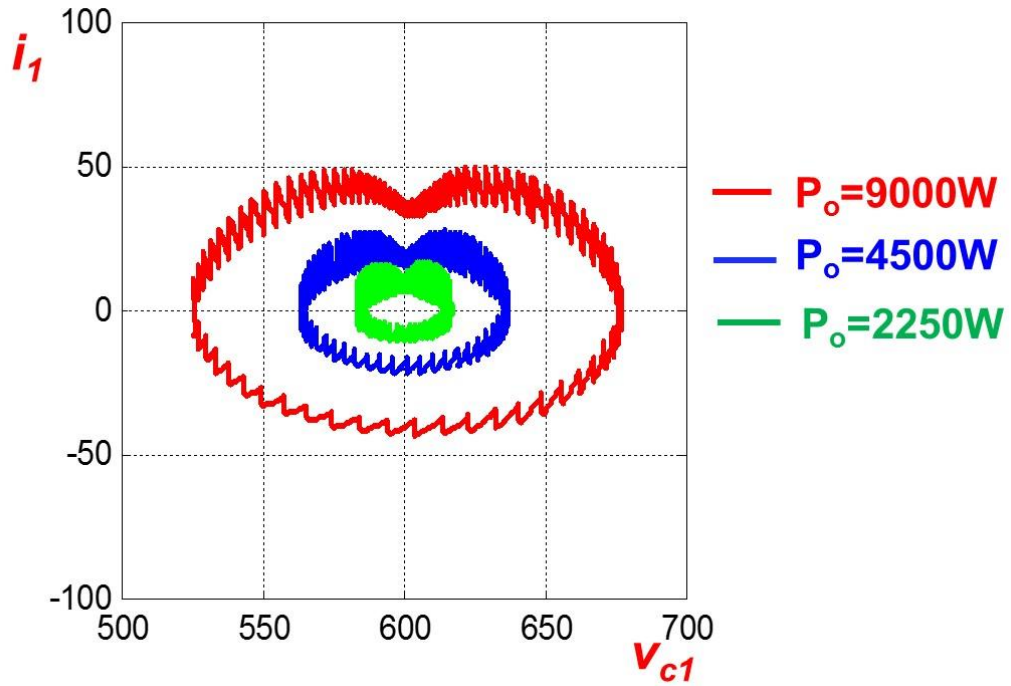


Fig.3. 4 State trajectory of  $i_1$  and  $v_{c1}$  with different power rating

Fig.3. 5 shows the 2D state trajectory in terms of the  $v_{c1}$  and  $v_{c2}$  planes and the voltage waveform. The state trajectories cross paths during one-line cycle, symptomizing the energy exchange between modules. The waveform and trajectory can be separated to two parts. In blue interval the voltage in upper and lower module change in different direction, that means when one increases the other one decreases. In red interval the voltage in upper and lower module change in same direction, when one increases or decreases the other one also increases or decreases.

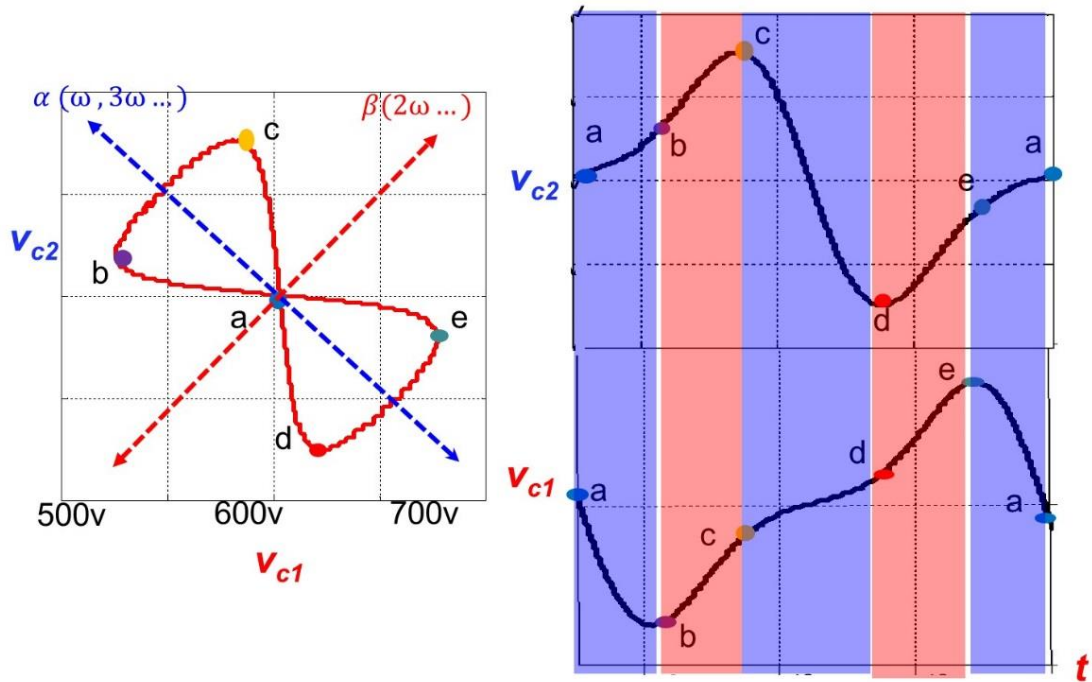


Fig.3. 5 2D state trajectory of the  $v_{c1}$  and  $v_{c2}$  planes and waveforms

To explain this phenomenon, two axes are defined; the  $\alpha$ -axis and the  $\beta$ -axis. The  $\alpha$ -axis denotes the energy storage related to odd-order harmonics, which is associated with the blue interval in waveform. On the other hand, the  $\beta$ -axis is related to even-order harmonics, which is associated with the red interval in waveform. The above statements are supported by examining (3.2) and (3.3). In (3.2) and (3.3), the fundamental and third-order harmonics are represented with the opposite sign, meaning energy exchanges between these two modules. The second-order harmonics are represented with the same sign, meaning energy is stored in the modules and eventually delivered out of the power phase.

If we use the power flows analysis in Fig.2. 14 as cross reference, we



---

could find that the  $\alpha$ -axis is related to power swapping between modules and the  $\beta$ -axis is related to power exchange between module and source or load.

### ***3.2 State Trajectory Analysis for Different Control Method***

In this sub-section, the proposed state-trajectory analysis is employed to evaluate the effectiveness of various control strategies with the intent of minimizing circulating energy and the bulk capacitor.

#### **Example 1: Simple control law**

The simple control law used in the previous section is employed here as the first example to illustrate the power flow analysis. As noted in Fig.2. 13, the module has a significant role in energy storage and transfer for the system. Fig.2. 14 and Table 2. 3 shows the relationship between the arm current and the associated module power, which is broken down in terms of dc, fundamental components and harmonics.

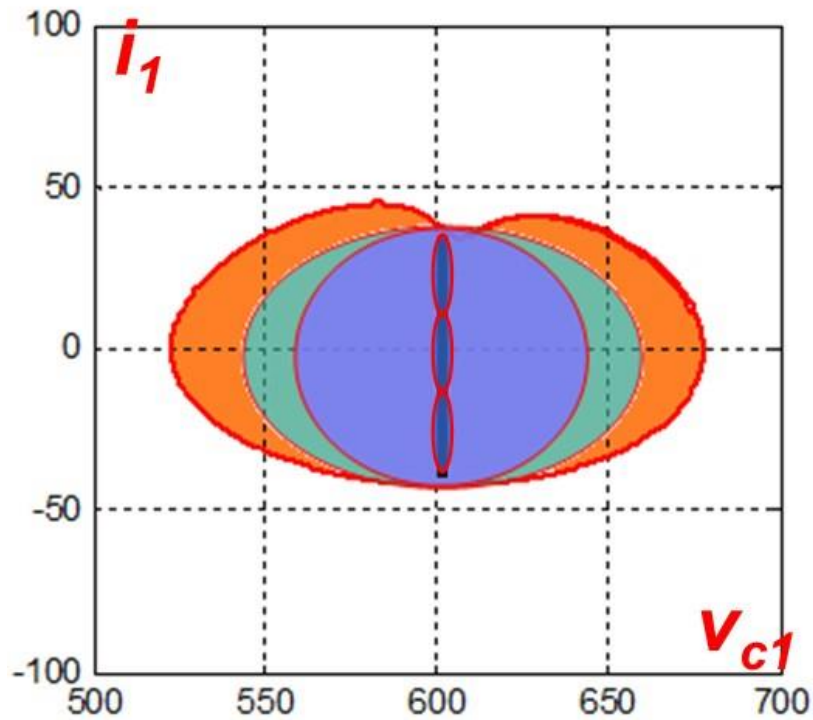


Fig.3. 6 power flow mapped state trajectory of  $i_1$   $v_{c1}$  in example 1

In Fig.3. 6, the areas that embody the state trajectory of  $i_1$  and  $v_{c1}$  in one line cycle of operation are represented by different colors, denoting different components of power outlined in the table. It should be noted that the state trajectory is biased along its x-axis with the 600V bias voltage, representing the dc average voltage of the capacitor. As shown in Table 2. 3, the sum of the dc power terms is zero. The dc power comes from the source to the module and is immediately inverted into ac and transferred to the load.

Since the module has to produce fundamental power, in the capacitor voltage there is a corresponding fundamental term. The fundamental term contributes the blue area of the state trajectory in Fig.3. 6, which also

relates to the blue terms in Table 2. 3. As explained above, this fundamental power switches to the lower arm, showing in Fig.2. 14. Since the net  $P_p(\omega t)$  is not zero, the capacitor needed to store energy is related to the fundamental frequency. The green area in Fig.3. 6 is caused by second-order harmonic power. This  $P_p(2\omega t)$  also produces the second-order voltage ripple in the capacitor. A portion of this power is associated with the green terms in Table 2. 3 and eventually transferred to the load, showing in Fig.2. 14. The second portion of  $P_p(2\omega t)$ , marked in orange, is the result of energy coming from source. This component of the power is further examined in Fig.2. 14.

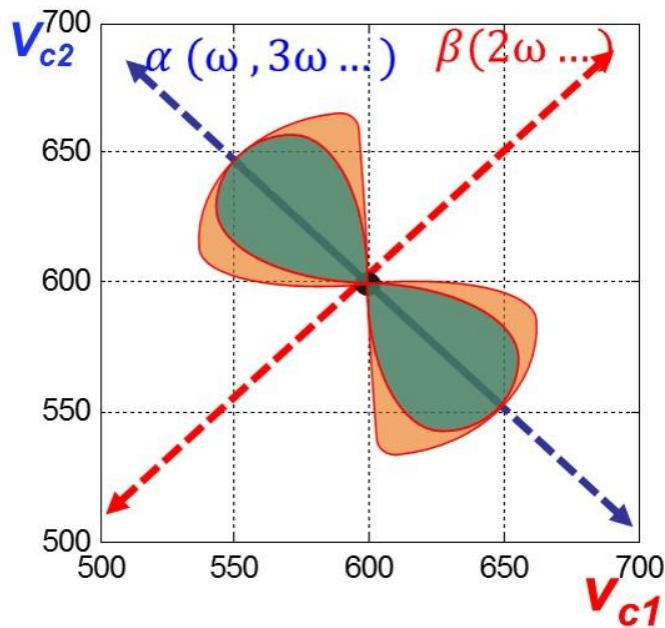


Fig.3. 7 power flow mapped state trajectory of  $i_1 v_{c1}$  in example 1

In Fig.3. 7, the fundamental power in Table 2. 3 and the fundamental component of the voltage contribute the blue line in the state trajectory. If

---

we consider both the upper arm and lower arm, the trajectory without any distance in  $\beta$ -axis means that power does not transfer out of phase nor transfer to the load nor source. This fundamental power only transfers between the arms. However, this power does make a voltage ripple in the capacitor, as shown in Fig.2. 143.

The green area in Fig.3. 7 represents the energy stored in the module and eventually transferred from the module to the load. It is colored in green in Table 2. 3 as well as in Fig.2. 14. Because this voltage ripple is a second-order harmonic, it extends the trajectory in the  $\beta$ -axis. As discussed above, the area indicates the power the phase arm contributes to the load.

Since the module also transfers power to the source, additional  $P_p(2\omega t)$  power is stored in the capacitor and indicated by the orange area in Fig.3. 7. and Table 2. 3. There is also a small amount of  $P_p(3\omega t)$  along the  $\alpha$ -axis. From the diagram, it can be seen that the fundamental component contributes most of the voltage ripple in the  $\alpha$ -axis.

#### Example 2: Zero harmonic current

A very popular control method is to eliminate the harmonic current with the idea of minimizing circulating current [36]. If the harmonic arm current is eliminated, the arm currents are:

$$i_1 = 0.5i_o + I_{dc} \quad (3.4)$$

$$i_2 = -0.5i_o + I_{dc} \quad (3.5)$$

With the harmonic current elimination, the voltage ripple in module capacitor can be reduced, showing in Fig.3. 8

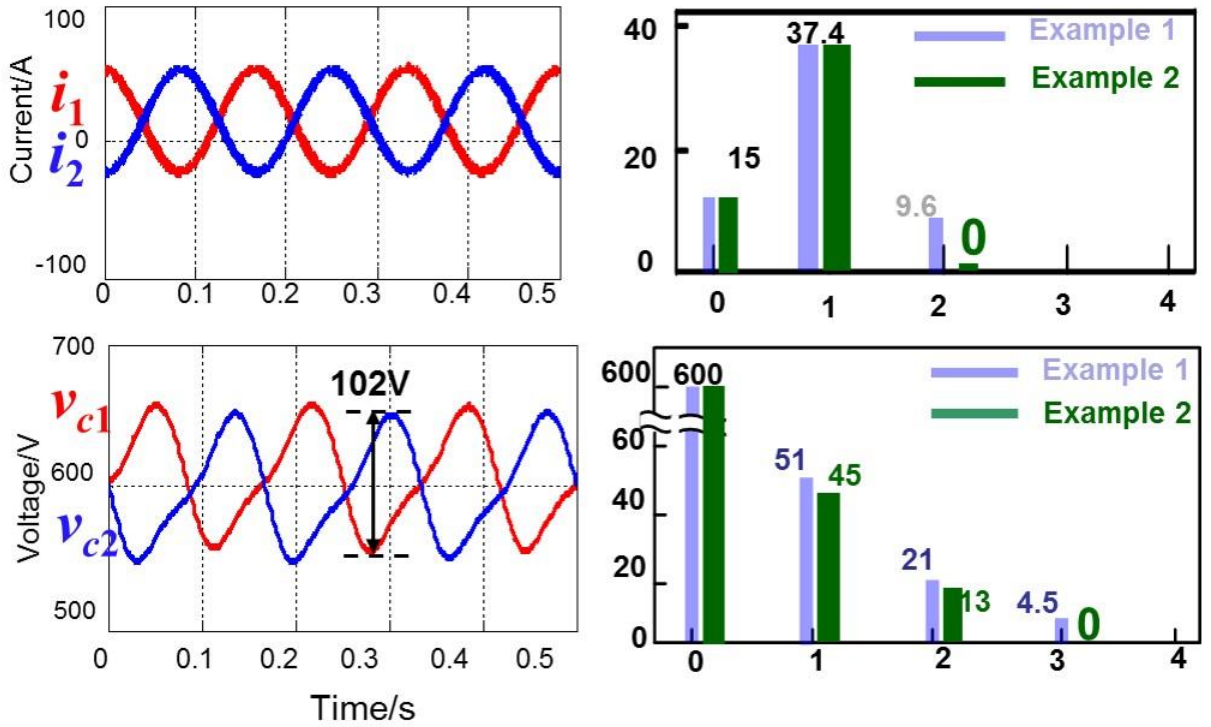


Fig.3. 8 simulation results of MMC with harmonic current elimination

From Fig.3. 8, we could notice that arm current has only DC part and fundamental part. As a result, the cap voltage ripple is also reduced. The fundamental, 2nd order are all smaller and the 3<sup>rd</sup> order harmonic is eliminated. Meanwhile, the phase modules power is defined as

$$p_p = \left(\frac{1}{2} I_o V_{dc} - I_{dc} V_o\right) \cos \omega t - \frac{1}{4} V_o I_o \cos 2\omega t \quad (3.6)$$

$$p_n = -\left(\frac{1}{2}I_oV_{dc} - I_{dc}V_o\right)\cos\omega t - \frac{1}{4}V_oI_o\cos 2\omega t \quad (3.7)$$

Using TABLE 3. 1 and Fig.3. 9, the function of the module power can be clearly explained. The module provides dc and  $P_p(2\omega t)$  power to the load and the  $P_p(\omega t)$  power switches between the upper and lower arms. In this example, the module no longer exchange power with the source.

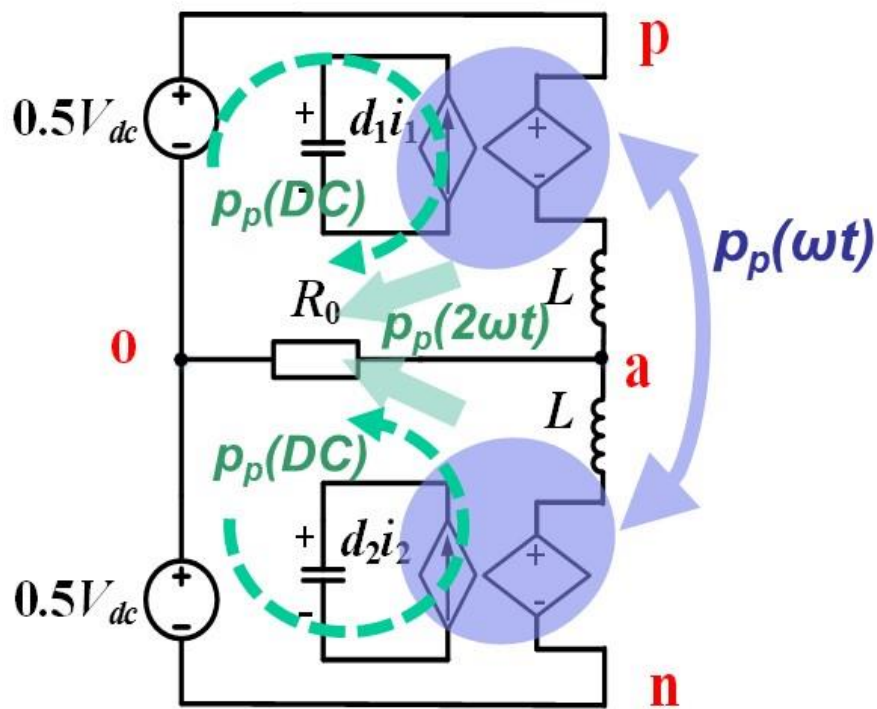


Fig.3. 9 Power transfer diagram for  $i_{har}=0$

TABLE 3. 1 POWER TRANSFER FOR  $I_{HAR}=0$

$i_1 \backslash P_p$	$p_p(DC)$	$p_p(\omega t)$	$p_p(2\omega t)$
$I_{dc}$	$\frac{1}{4}V_o I_o$	$-I_{dc}V_o$	
$\frac{1}{2}I_o \cos\omega t$	$-\frac{1}{4}V_o I_o$	$\frac{1}{2}I_o V_{dc}$	$-\frac{1}{4}V_o I_o$

Further details of the power storage and transfer can be examined using the state plans. In Fig.3. 10, the blue area is a result of fundamental power  $P_p(\omega t)$ , whose support module produces power that switches with the lower arm. The green area is caused by the second-order term  $P_p(2\omega t)$ . This component is needed to provide second-order power to the load.

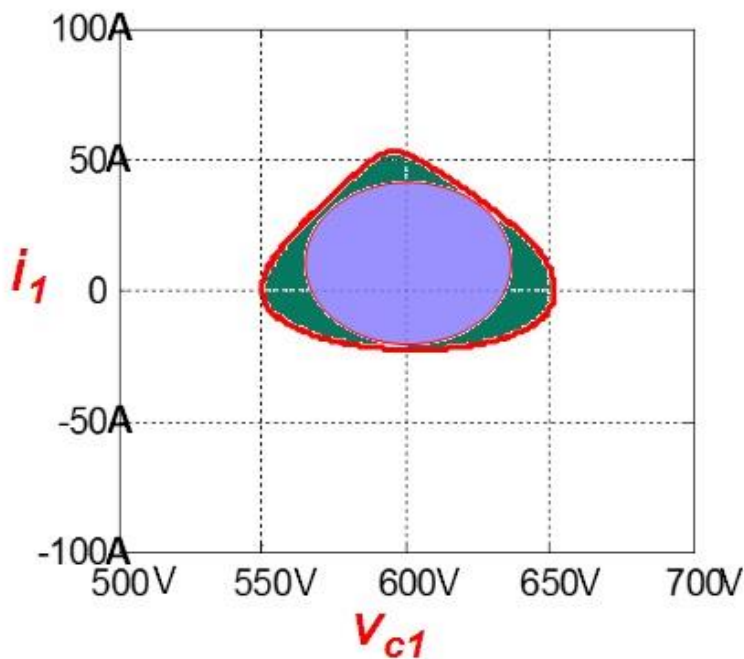


Fig.3. 10 2D state trajectory of  $i_1$  and  $v_{c1}$  with colored areas for  $i_{har}=0$

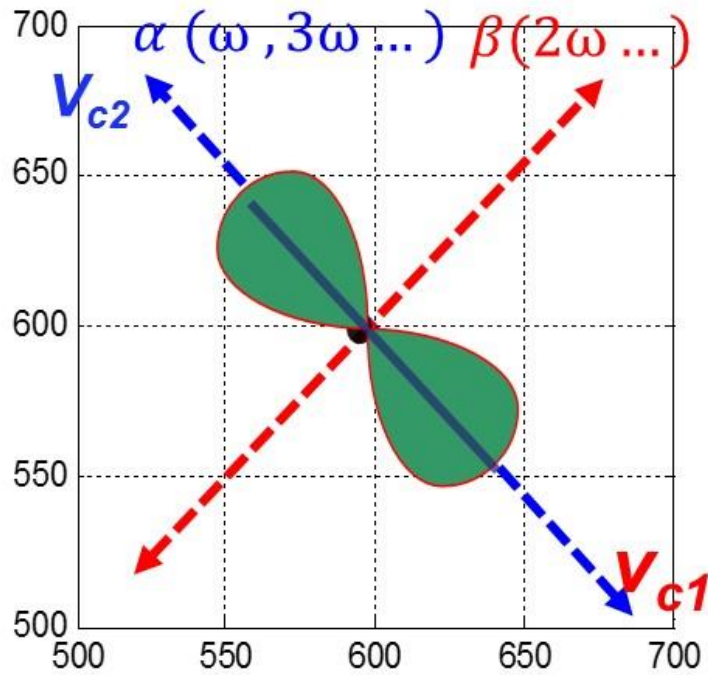


Fig.3. 11 2D state trajectory of vc1 and vc2 with colored area for ihar=0

Fig.3. 11 shows that the fundamental voltage extends the trajectory in the  $\alpha$ -axis, which causes the energy exchange between the two modules, denoted by the blue line. The green area is caused by the second-order voltage, which extends the trajectory in the direction of the  $\beta$ -axis. This area represents the energy stored in the capacitor related to  $P_p(2\omega t)$ , which is transferred to the load.

Compared with Example 1, the area enclosed by the state trajectory is smaller. Significant reduction of  $\beta$  energy and small reduction of  $\alpha$  energy. Since the module no longer needs to store energy that is eventually transferred back to the source, the capacitor voltage ripple is reduced. In this example the module still needs to store energy related to the



fundamental frequency and its second-order harmonic.

### Example 3: Second-order harmonic current injection

As discussed above, the module supplies second-order harmonic power to the load. If a proper amount of the second-order current is injected, the module may not need to store the second-order harmonic-related energy [36]. The proposed second-order harmonic current injection is:

$$i_{har} = I_{dc} \cos 2\omega t \quad (3.8)$$

With this harmonic current injection, the voltage ripple in module capacitor can be reduced, showing in Fig.3. 8

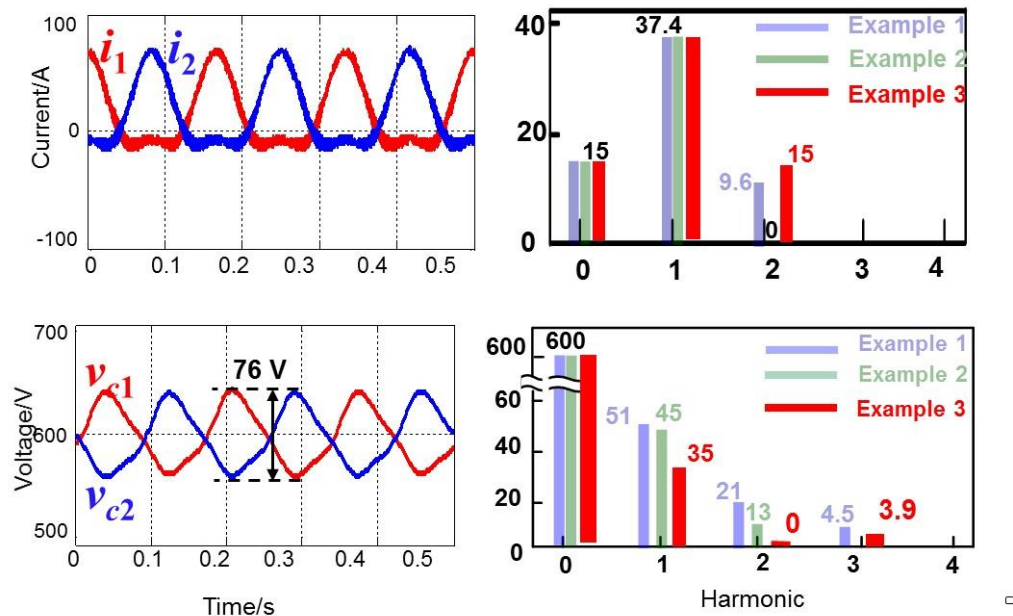


Fig.3. 12 simulation results of MMC with 2<sup>nd</sup> order harmonic injection

With the harmonic current as 2<sup>nd</sup> order, the cap voltage ripple is

---

reduced. In cap voltage, the fundamental part is reduced, the 2<sup>nd</sup> order part is eliminated, but introduced a small 3<sup>rd</sup> order part.

the second-order component of the module power as shown in (3.9) and (3.10) will cancel out each other. That means the module does not provide power to the load or to the source. The power equations are simplified significantly:

$$p_p = \left(\frac{1}{2}I_o V_{dc} - I_{dc} V_o + \frac{1}{2}I_{dc} V_o\right) \cos \omega t + \frac{1}{2}I_{dc} V_o \cos 3\omega t \quad (3.9)$$

$$p_n = -\left(\frac{1}{2}I_o V_{dc} - I_{dc} V_o + \frac{1}{2}I_{dc} V_o\right) \cos \omega t - \frac{1}{2}I_{dc} V_o \cos 3\omega t \quad (3.10)$$

Using Table 3. 2 and Fig.3. 13, the function of module power flow can be clearly explained. The module only needs to store the  $P_p(\omega t)$  needed to switch between the upper and lower arms. All the load power comes from the source. From Table 3. 2, we can observe that only the odd-order power components exist in the module.

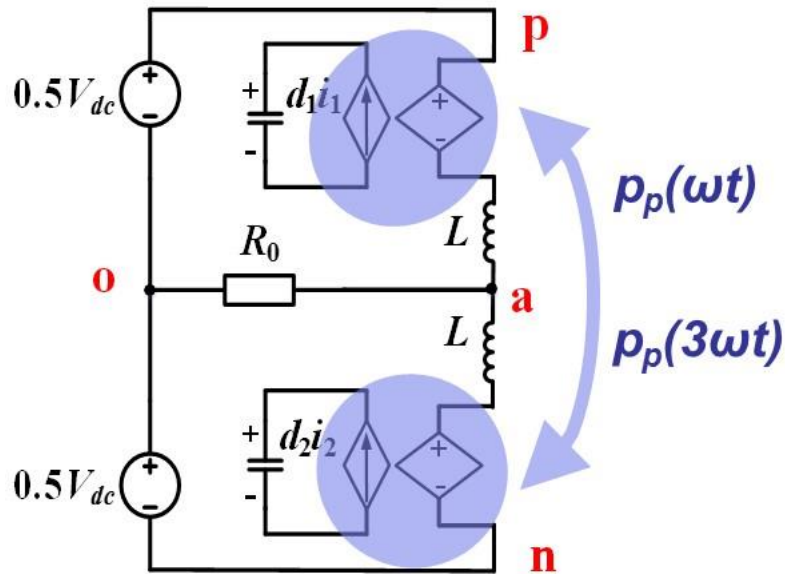


Fig.3. 13 Power transfer diagram for second-order current injection

TABLE 3. 2 POWER TRANSFER FOR SECOND-ORDER CURRENT INJECTION

$i_1 \backslash p_p$	$p_p(DC)$	$p_p(\omega t)$	$p_p(2\omega t)$	$p_p(3\omega t)$
$I_{dc}$	$\frac{1}{4} I_o V_o$	$-I_{dc} V_o$		
$\frac{1}{2} I_o \cos \omega t$	$-\frac{1}{4} I_o V_o$	$\frac{1}{2} I_o V_{dc}$	$-\frac{1}{4} I_o V_o$	
$I_h \cos 2\omega t$		$-\frac{1}{2} I_{dc} V_o$	$\frac{1}{4} I_o V_o$	$-\frac{1}{2} I_{dc} V_o$

Details of the power storage and transfer can be examined using the state planes. In Fig.3. 14, the blue area is further reduced compared to Example 2. The capacitor voltage consists of only the fundamental and third-order harmonic voltages.

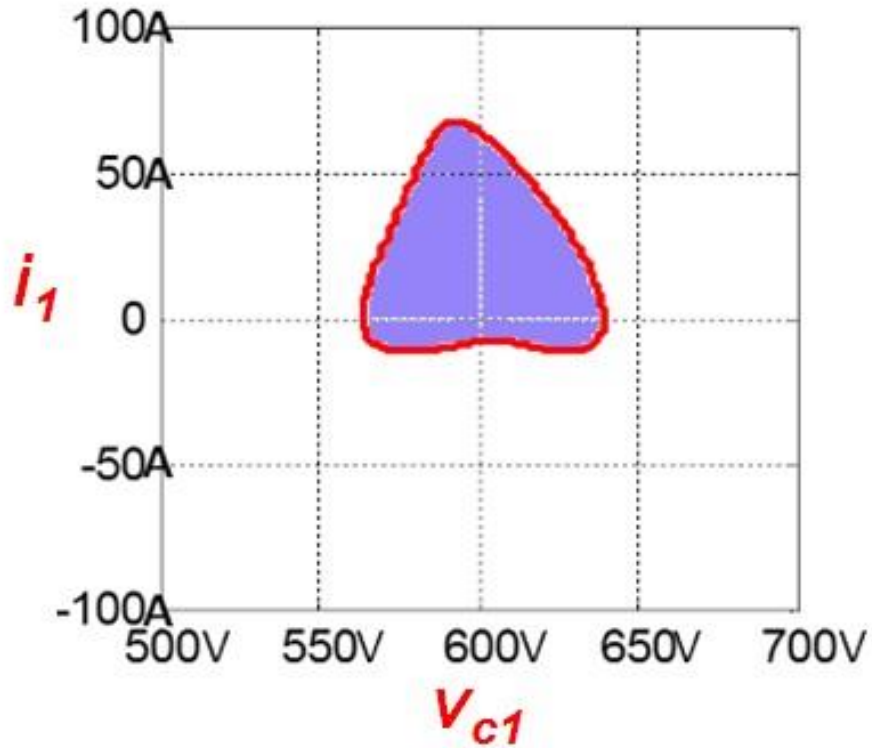


FIG.3. 14 2D state trajectory of  $i_1$  and  $v_{c1}$  with colored area representing second-order harmonics

Fig.3. 15 clearly shows in this case the state trajectory only travels along the  $\alpha$ -axis; thus no even-order harmonics exists. As discussed above, this means that no power transfers out of the phase module to the source or load. The only circulating power that exists is  $P_p(2\omega t)$  switching between the arms. Moreover, due to the strong injected second order current, the circle loop is not round like.

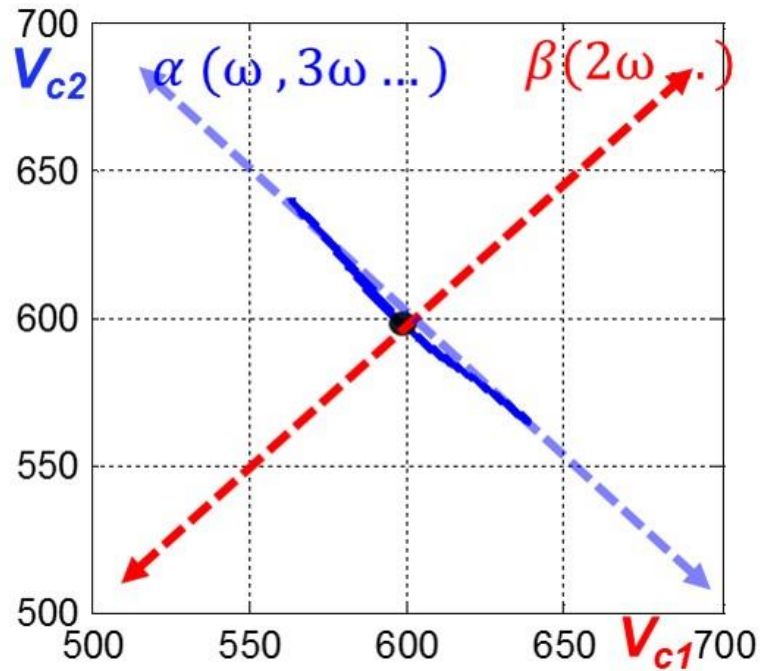


Fig.3. 15 2D state trajectory of  $v_{c1}$  and  $v_{c2}$  for second-order current injection

Compared with the previous cases, this case is more promising. However, the main issue remains that the modules still need to store and transfer line-frequency-related circulating energy; thus the capacitor bank remains bulky.

#### Example 4: Controlling the modulation index

Observing the module power (3.9) (3.10), we could find that there is only odd order harmonic power which contribute all the voltage ripple. In (3.9),(3.10) the module power is a function of  $V_{dc}$ ,  $V_o$ ,  $I_o$  and  $I_{dc}$ . Meanwhile, those four variables have relationship which is associated with the modulation index  $M$ , as following representation:

$$M = 2V_o / V_{dc} \quad (3.11)$$

Substitute (3.11) in to (3.9) and (3.10), the module power equation can be rewritten as:

$$\begin{cases} p_p = \left(\frac{1}{2M} - \frac{3}{8}M\right)I_oV_o \cos \omega t - \frac{1}{8}MI_oV_o \cos 3\omega t \\ p_n = -\left(\frac{1}{2M} - \frac{3}{8}M\right)I_oV_o \cos \omega t + \frac{1}{8}MI_oV_o \cos 3\omega t \end{cases} \quad (3.12)$$

The expression of module power is a function of modulation index M. When M changes, the power and voltage ripple also change, as shown in Fig.3. 16.

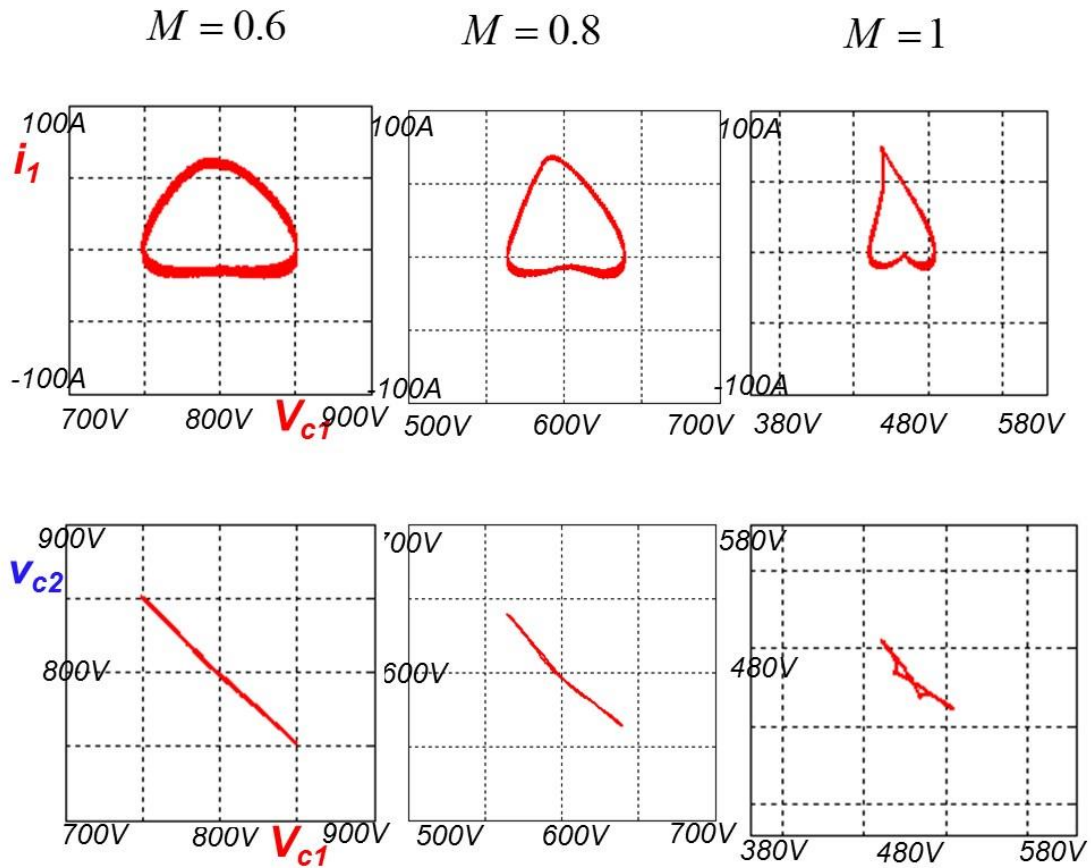


Fig.3. 16 State plane with changing modulation index

As shown in Fig.3. 16, when M increases, the  $\alpha$  energy decreases, that

---

can be also examined in (3.12). Our team have recently proposed a new control strategy of controlling modulation index  $M$  while still injecting the second-order harmonic current in the same way as Example 3. By over-modulation one can further reduce the fundamental component of circulating energy. If  $M = 1.15$ , the fundamental component of energy can be totally eliminated and the capacitor size drastically reduced. Since the modulation index is always less than one in the half-bridge module, the concept can only be implemented in the full-bridge topology. Analyzing the module power equations in the previous case, with  $M=1.15$  they can also be written as:

$$\begin{cases} p_p = -\frac{1}{8}MI_oV_o \cos 3\omega t \\ p_n = \frac{1}{8}MI_oV_o \cos 3\omega t \end{cases} \quad (3.13)$$

However, in half bridge module, the modulation index has limitation. It cannot larger than 1. In order to increase  $M$  to 1.15, full bridge module could be employed. As shown in Fig.3. 17. with full bridge module, the modulation index is limitation free.

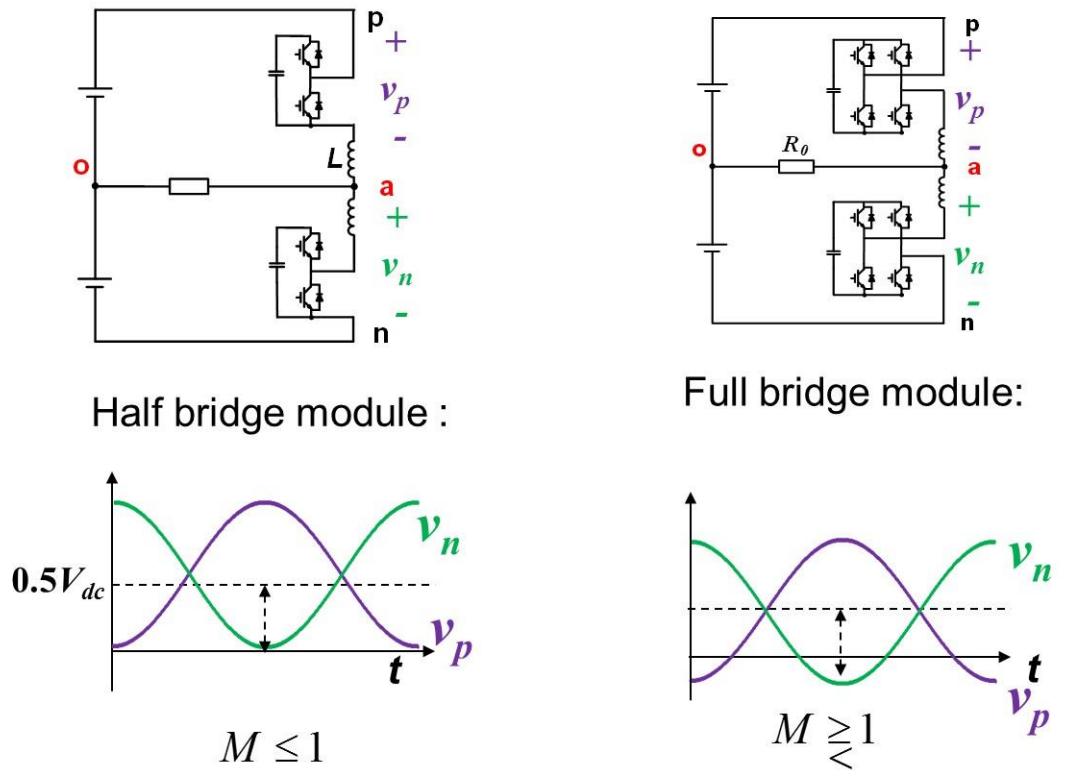


Fig.3. 17 modulation index control realized with full bridge module

With this modulation index control, the voltage ripple in module capacitor can be reduced a lot, showing in Fig.3. 18

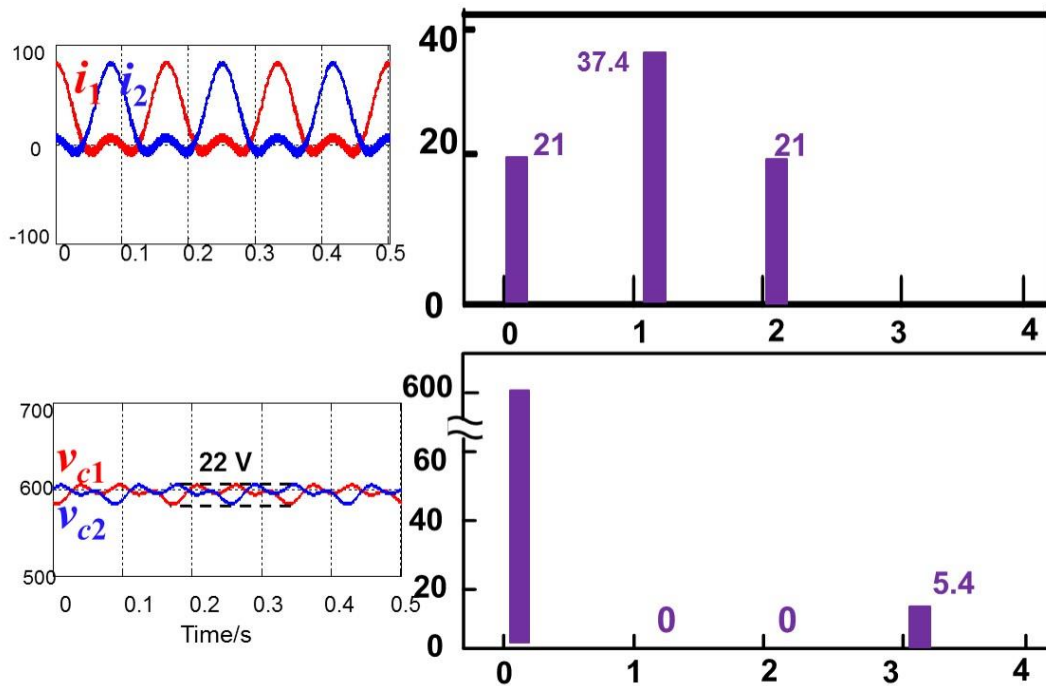


Fig.3. 18 simulation results for modulation index control



In cap voltage, the fundamental part is zero, the 2<sup>nd</sup> order part is eliminated, still there is a small 3<sup>rd</sup> order part.

Under proposed control method, there is only a small amount of circulating energy related the third-order harmonic, and it switches between the upper and lower arms. From TABLE 3. 3 and we can observe that most of the power terms are equal to zero; the only term left is a small amount of third-order power.

Table 3. 3 Power transfer for Modulation Index control

$i_1 \backslash p_p$	$p_p(DC)$	$p_p(\omega t)$	$p_p(2\omega t)$	$p_p(3\omega t)$
$I_{dc}$	$\frac{1}{4} I_o V_o$	$-I_{dc} V_o$		
$\frac{1}{2} I_o \cos \omega t$	$-\frac{1}{4} I_o V_o$	$\frac{1}{2} I_o V_{dc}$	$-\frac{1}{4} I_o V_o$	
$I_h \cos 2\omega t$		$-\frac{1}{2} I_{dc} V_o$	$\frac{1}{4} I_o V_o$	$-\frac{1}{2} I_{dc} V_o$

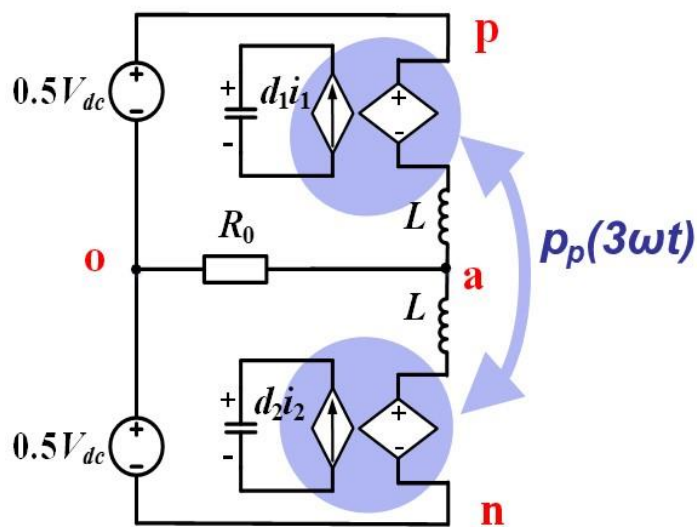


Fig.3. 19. Power transfer diagram for M = 1.15

Fig.3. 20 illustrates that the area embodied by the state trajectory is very small and related only to the third-order harmonic voltage.

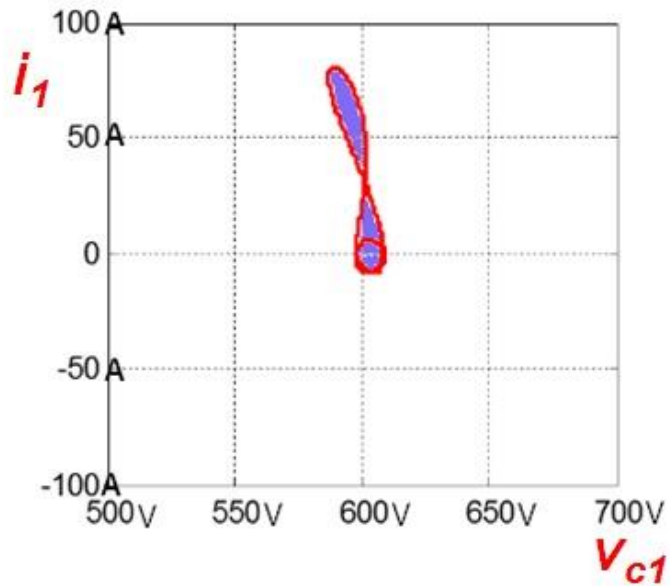


Fig.3. 20 2D state trajectory of  $i_1$  and  $v_{c1}$  for  $M = 1.15$

Fig.3. 21 shows the state trajectory of  $v_{c1}$  and  $v_{c2}$ . The small state trajectory is caused by the small third-order voltage. There is no fundamental or second-order harmonic. The  $\alpha$  energy and  $\beta$  energy are both reduced near zero.

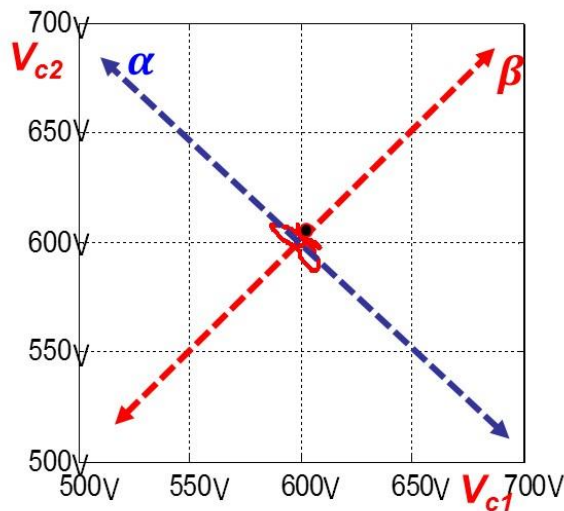


Fig.3. 21 2D state trajectory of  $v_{c1}$  and  $v_{c2}$  with colored area for  $M = 1.15$

Compared with the previous cases, this case is much better. The fundamental ripple is eliminated and there is only small third order harmonic in capacitor voltage, whose effect is very limited. From the state plane we could notice that in the Fig.3. 21, the voltage is fluctuating around the middle point, that means most of the circulating power is eliminated in this circuit.

In Fig.3. 22. a summary of proposed examples is plotted. It is obvious that in our final design, the modulation index control, the capacitor voltage ripple can be significantly reduced and the circulating power in this circuit is almost eliminated.

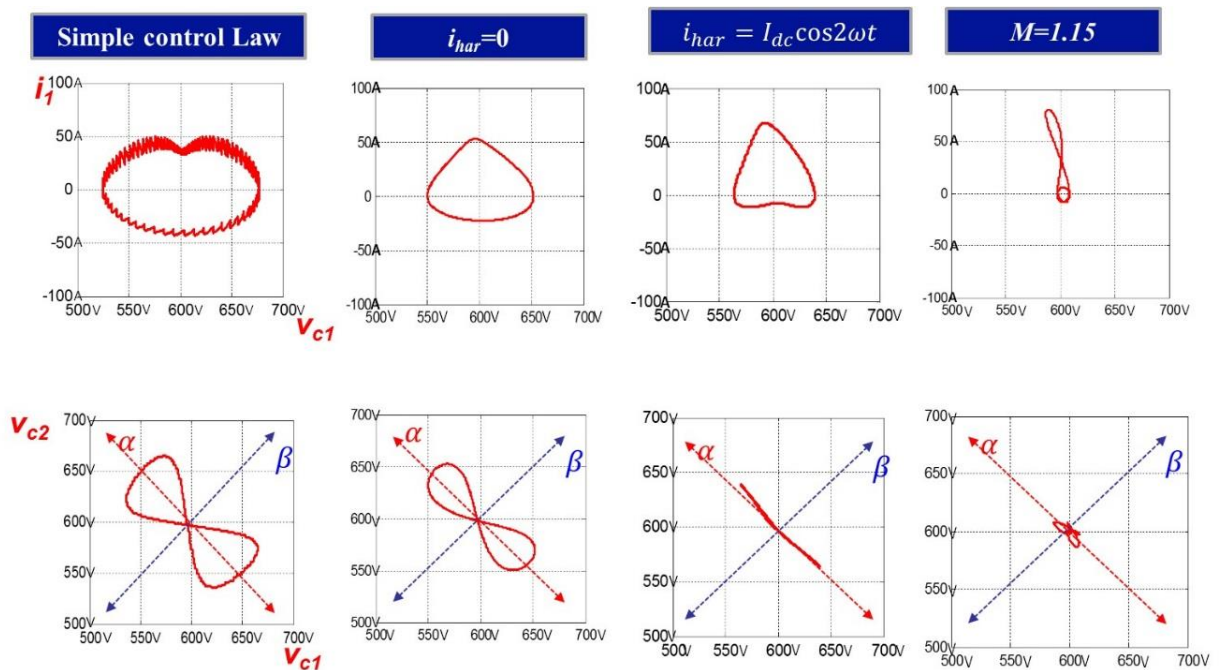


Fig.3. 22 comparison of state trajectory for different control strategies

---

### Example 5: High-frequency injection for three-phase MMC

A more complicated case, the high frequency injection method was proposed in [37] to reduce the capacitor voltage ripple. It was employed to demonstrate the start-up of an induction motor with quadratic-torque loads. However, it only considers the dc and fundamental components in the branch current and ignores the second-order components, so the power flow processes are very complex.

The author injected a high-frequency common-mode voltage in the neutral point of the three-phase load. The structure of this method is shown in Fig.3. 23. The high-frequency common-mode voltage is added between point m and point o. This high-frequency voltage injection makes it possible to eliminate the low-frequency harmonic power in the module.

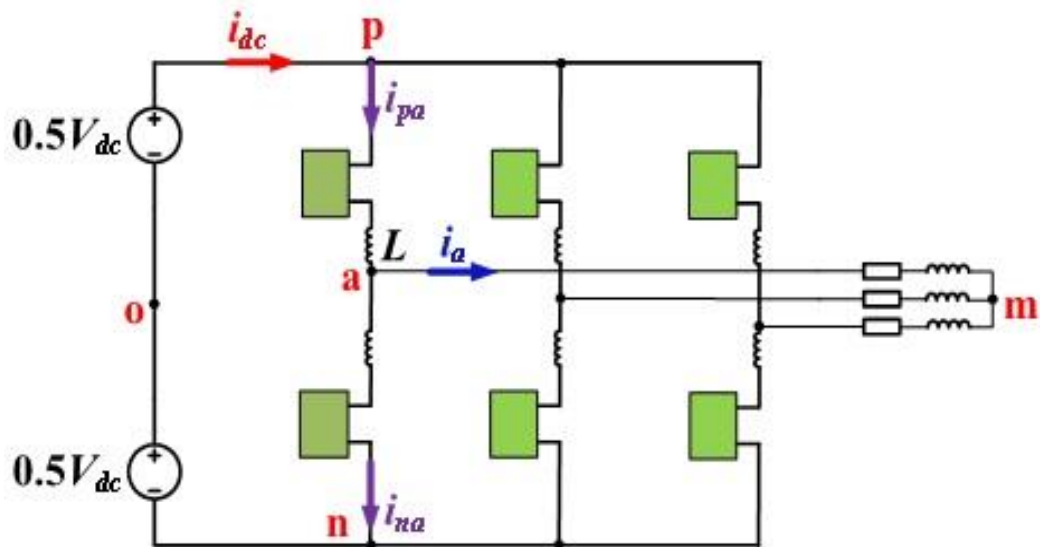


Fig.3. 23 Three-phase MMC for high-frequency common-mode voltage injection

---

The power flow in the proposed method is rather complex to analyze, but using the proposed state trajectory can help us gain some insight into this approach.

Based on the concept in [37], a simulation is done with the parameters in Table 3. 4 and the structure in Fig.3. 23

Table 3. 4 Parameters for High-Frequency Injection

DC source voltage	600 V
Line frequency	60 Hz
Arm inductance	2 mH
Modulation Index	0.4
SM capacitance	750 $\mu$ F
Switching frequency	5 kHz
Load Resistor	3.2 Ohms
Magnitude of the common-mode voltage	162V
Frequency of the common-mode voltage	480 Hz

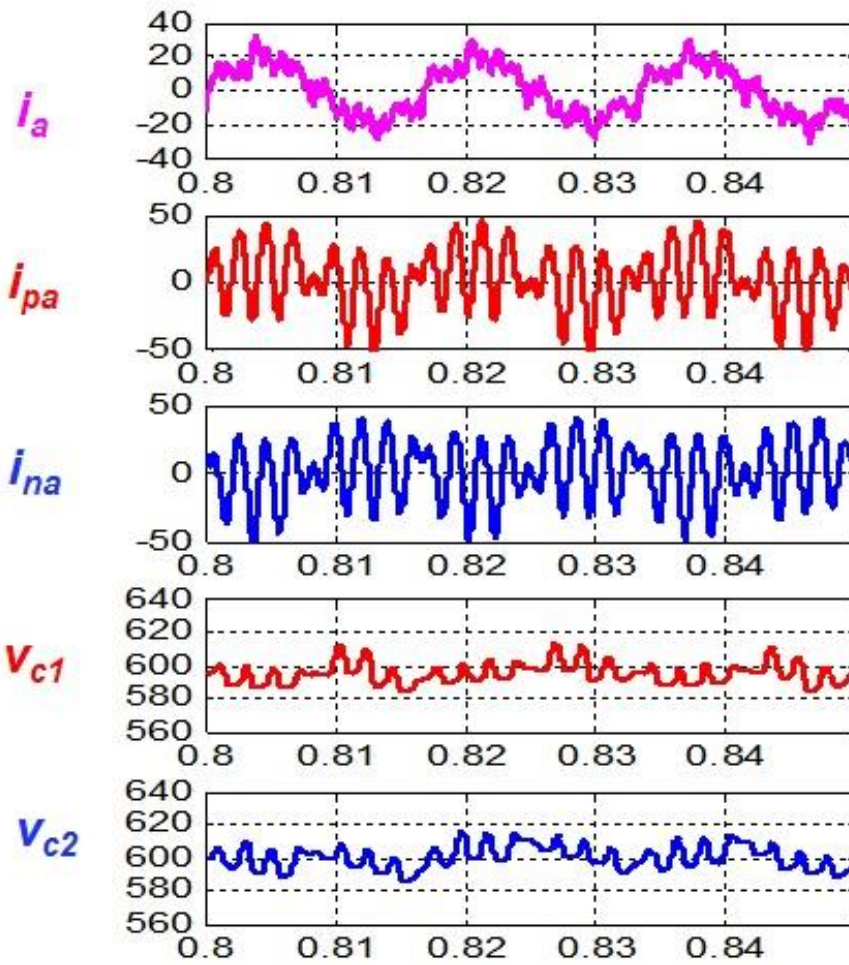


Fig.3. 24 Simulation results of high-frequency common-mode voltage injection

The simulation results waveforms in Fig.3. 24 show that the high-frequency capacitor voltage ripple dominates the voltage fluctuation. The low-frequency voltage ripple is suppressed. The state trajectories of this simulation are plotted in Fig.3. 25.

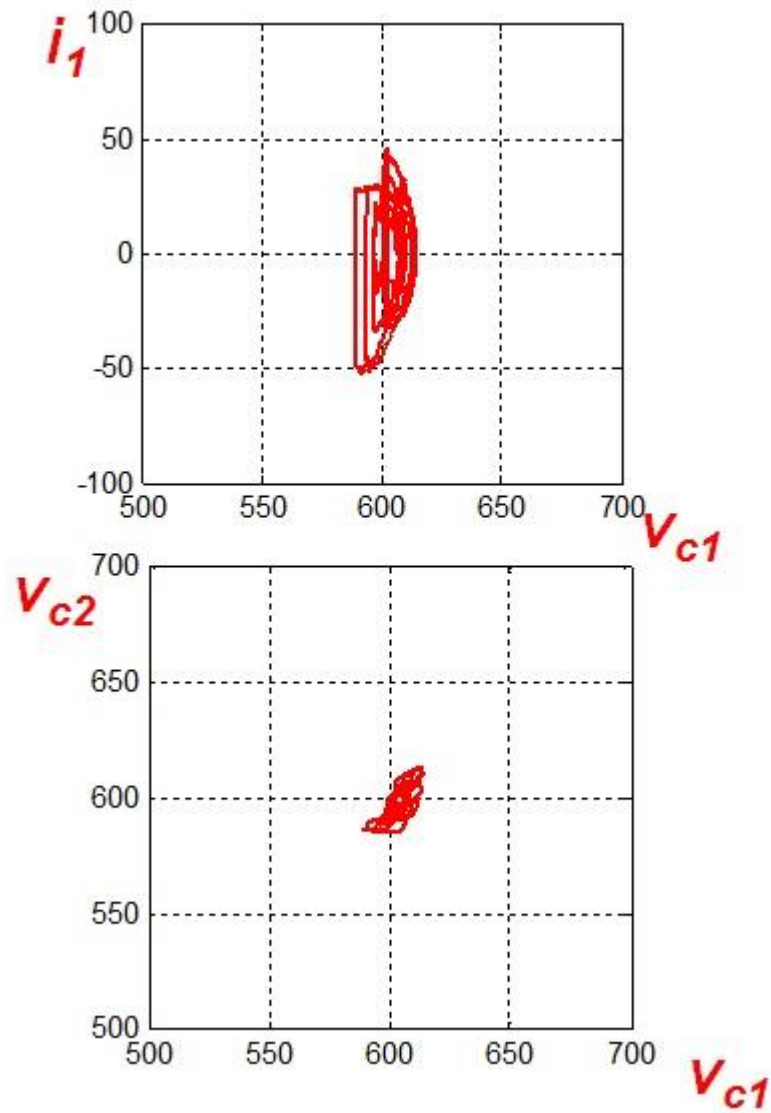


Fig.3. 25 State trajectory comparison of high-frequency injection and over-modulation

Unlike Example 4, here the high-frequency injection method encircles the quiescent point numerous times while the over-modulation method only encircles it once in a line cycle. In both cases, the fundamental and second-order line frequency components are invisible.

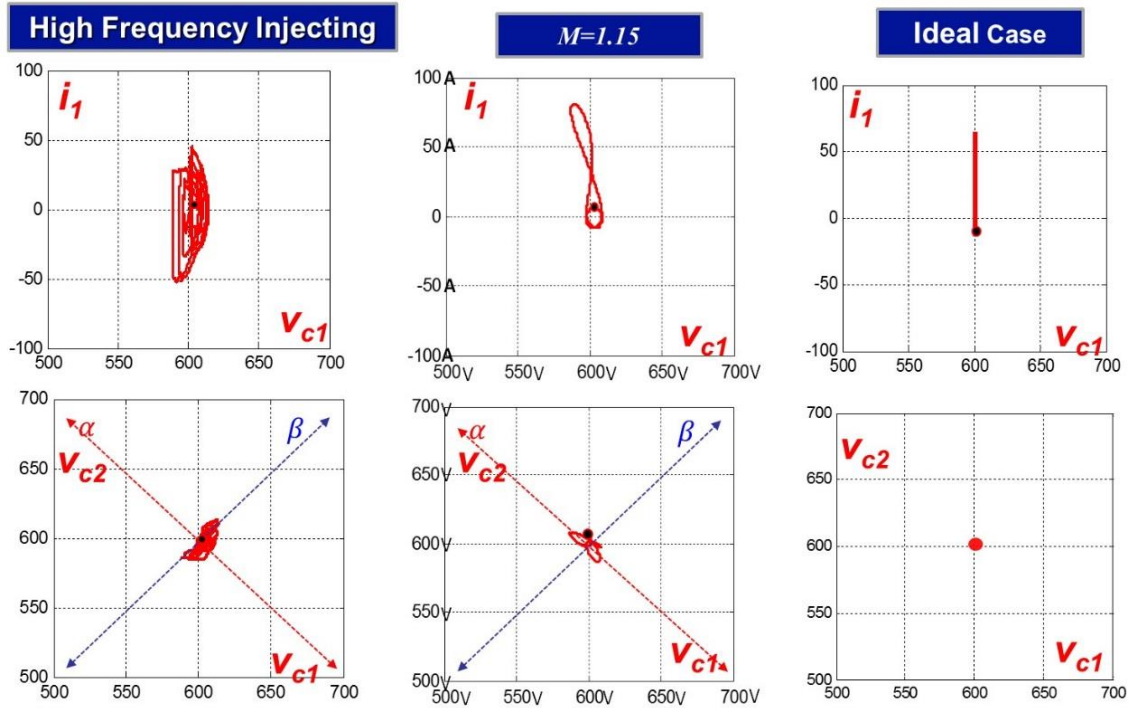


Fig.3. 26 comparison of high frequency injection, modulation index control and ideal case

Fig.3. 26 plots three state plane for the best solutions and ideal case. The high frequency injection method can suppress the voltage ripple a lot, especially the low frequency harmonic voltage can be eliminated. However, due to the injected high frequency common mode voltage, in one-line cycle, the current fluctuates many times, meaning large conduction loss. On the other hand, the modulation index control can provide an even smaller voltage ripple with low frequency current and voltage fluctuation. Comparing with the ideal case without any voltage ripple, the modulation index control method can offer a near-perfect result.



---

## Chapter 4 Verification of Concept

### 4.1 Concept extension to multi modules

In industry application, a MMC system contains numerous of sub-modules. All the modules share the high DC link voltage. A scale downed three phase MMC with 12 modules per arm is demonstrated in Fig.4. 1 for implementing the concept to real case. The parameters are shown in Table 4. 1 The sub-modules in this circuit can be half bridge or full bridge.

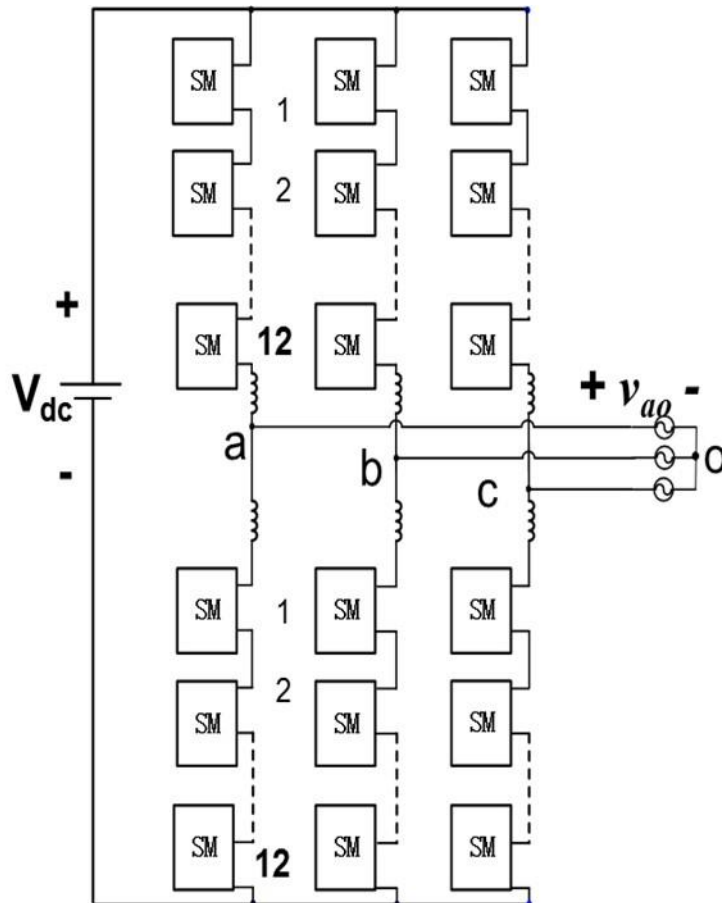
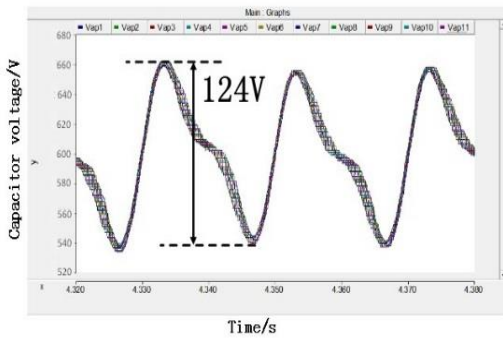


Fig.4. 1 Circuit Structure for MMC with 12 module per arm

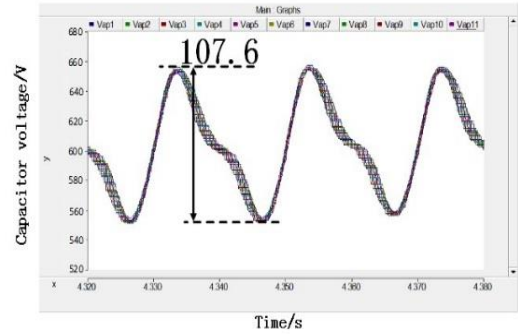
Table 4. 1 Parameters for simulation with 12 modules per arm

DC bus voltage	7.2kV
Power rating	1MW
Line frequency	60Hz
Arm inductor (L)	4.8mH
Module capacitance	900 $\mu$ F
Switching frequency	4800Hz
Modules per arm	12

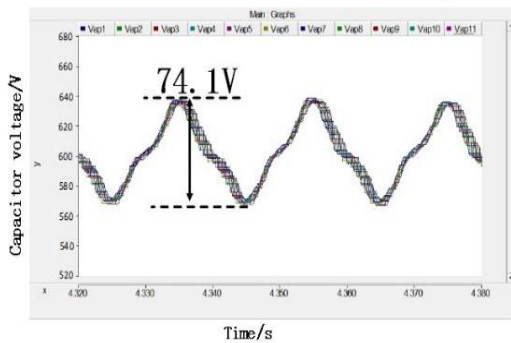
Example 1: No Cir. Current Control



Example 2: Cir. Current Suppression



Example 3: 2<sup>nd</sup> order Cir. Current Injection



Example 4: Full-bridge MMC

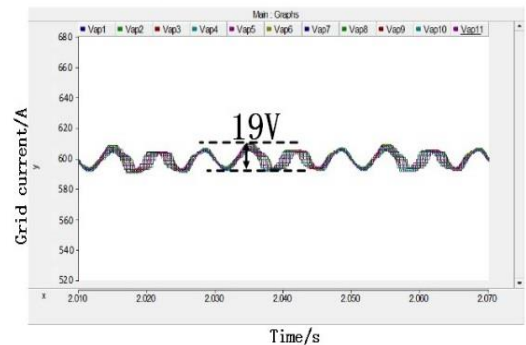


Fig.4. 2 Simulation results for proposed control methods

Fig.4. 2 describes the simulation results of proposed voltage ripple suppression methods. By observing the results, we could notice that the

concept of modulation index control and the other control methods work well for multi modules case and they all can reduce the capacitor voltage ripple. Fig.4. 3 gives us the summary of voltage ripple of the examples proposed.

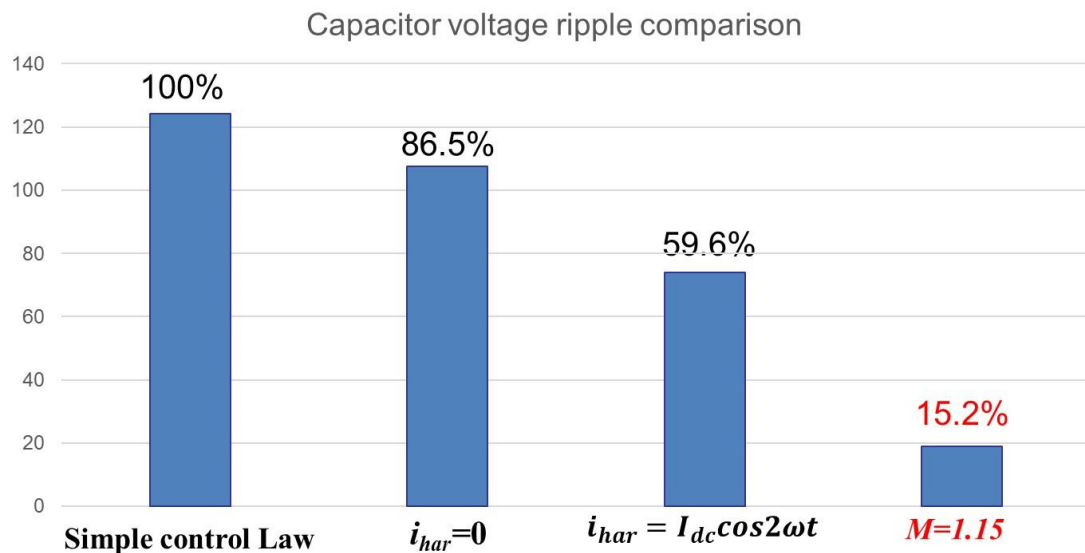


Fig.4. 3 summary of voltage ripple of the different control method

Base on the results in Fig.4. 3, with modulation index control, the voltage ripple can be reduce 85%. That means with the same voltage ripple tolerance standard, the capacitance can be reduced 85%. Therefore, in this simulation circuit, the 900  $\mu\text{F}$  capacitance can be replaced with 135  $\mu\text{F}$ . For industry application, small capacitance means saving money and space. Especially for the MMC built in the offshore platform, the volume of bulky capacitor is a significant issue.

However, in the design 4, in order to implement a modulation index equals 1.15, full bridge modules have to be used. Hence, the conduction loss is increased in this case. Base on the information of a 1.2kV IGBT

from SEMTIRON (SKM400GA12V), the semiconductor loss evaluations of different designs has been done. A preliminary loss comparison under different control methods is given in Fig. 11.

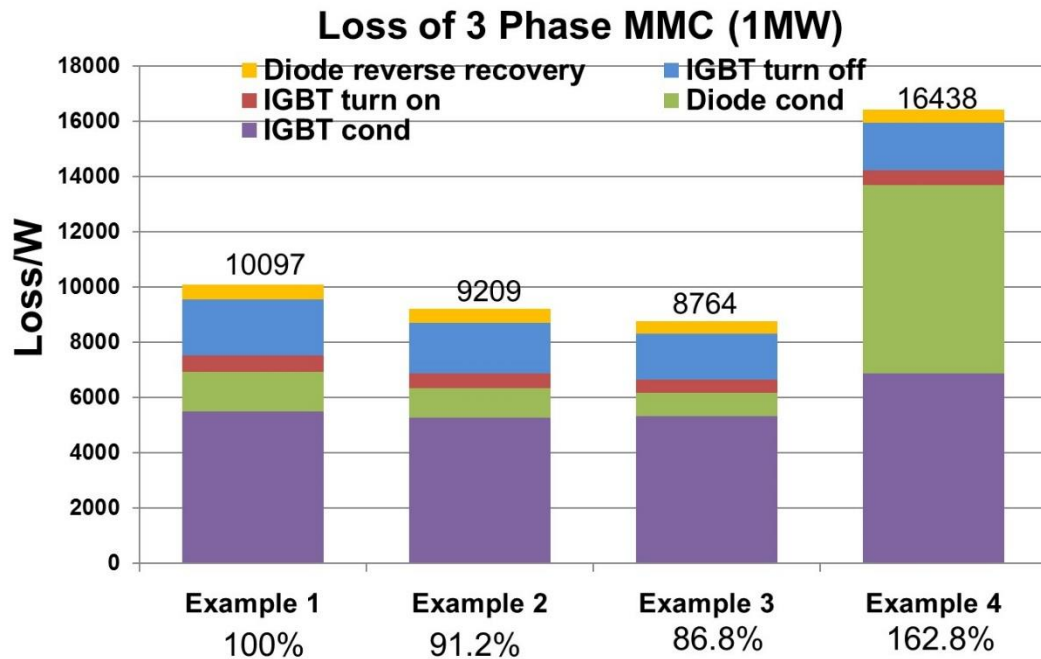


Fig.4. 4 semiconductor loss evaluations

By observing Fig.4. 4, one can find that the loss of design 2 is about 10% less than design 1. And in design 3 the loss is reduced further. However, the design 4 increases the loss to 162.8% of the first design. Most of the increased loss comes from diode conduction loss.

#### ***4.2 Scaled down hardware of MMC***

Computer simulation enlightens us to figure out new control and analysis aspect. And our concepts are all verified on simulation. However, in real case, there are unexpected problems and challenges. A scaled down hardware of three phase MMC system is built to verify the concept and

provide us inspiration of research outlook. The structure of the prototype hardware is shown in Fig.4. 5.

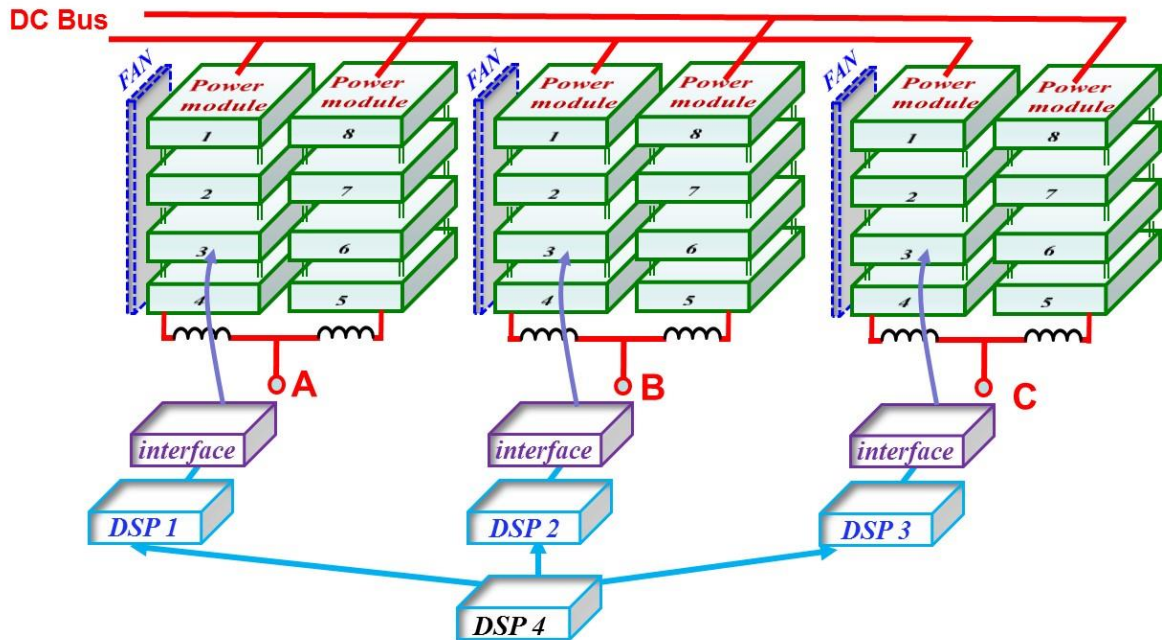


Fig.4. 5 Structure of Scaled down MMC hardware

Shown as in Fig.4. 5, the system is a converter connected between DC bus and AC output. It has 24 sub-modules which are separated to three phases, meaning 8 modules per phase and 4 modules per arm. Each phase has a DSP control board for most of the individual controlling. Moreover, there is also a master control board to deal with the communication issue between three phase and to give some general control order. The parameters of this system are in Table 4. 2

TABLE 4. 2 PARAMETERS OF SCALED DOWN MMC HARDWARE

DC bus voltage	600V
DC current	3 A
Power rating	5.4 kW
Line frequency	60 Hz
Arm inductor (L)	0.3mH
Module capacitance	1200 $\mu$ F
Switching frequency	Up to 10kHz
Modules per arm	4
Load resistance	18 Ohm

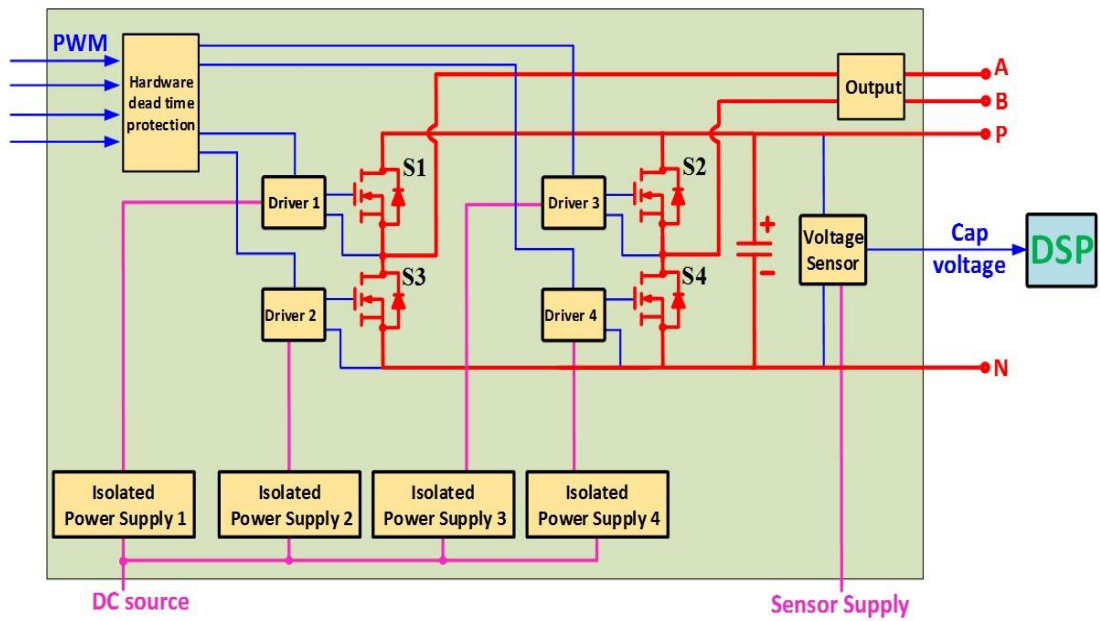


Fig.4. 6 circuit of sub-module power stage

The schematic of one sub-module is shown in Fig.4. 6. Four MOSFET are driven by four individual gate driver which are supported by four isolated power supply. The PWM signal are secured by the hardware protection which can provide the dead time protection and make sure the signals of upper switch and lower switch are complementary. The module has two output mode. When P and N are connected to the arm, the module works as half bridge. When A and B are connected to the arm, it works as Full bridge. The voltage sensor on power stage can probe the capacitor voltage of module and send the information to control board.

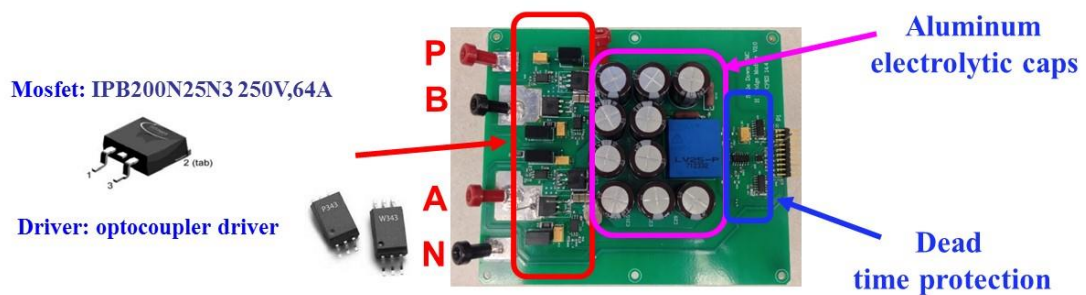


Fig.4. 7 Picture of one sub-module

The picture of one sub-module is shown in Fig.4. 7. Due to the DC bus voltage is 600V and there are 4 modules per arm, the capacitor DC bias voltage is 150V. Moreover, the used MOSFET should have enough voltage margin for the safety and stability of the system. Therefore, the MOSFET we use is IPB200N25N3 with the voltage rating 250V and 64A current tolerance. The power loop and signal loop are settle on two side of the board to avoid the interference.

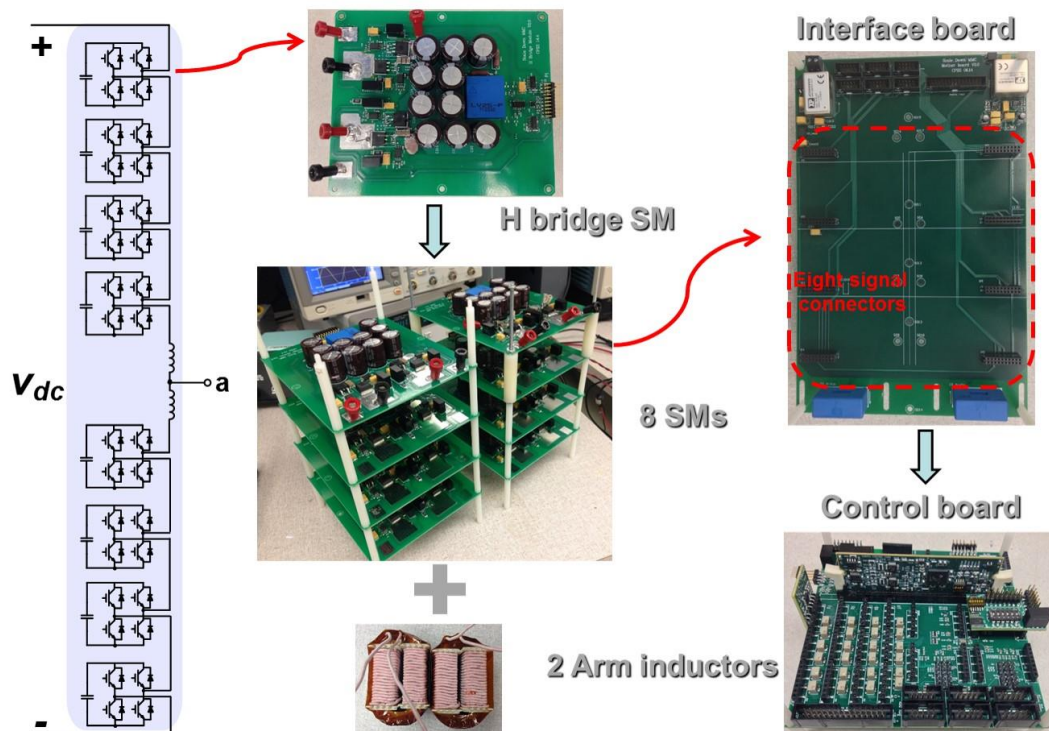


Fig.4. 8 one phase leg of the scaled down hardware MMC

Fig 4.8 shows one phase leg of the MMC hardware. Each arm has four modules and all the control and sensor signals are transferred through an interface board to the control board. The interface board also offers low voltage power to modules and control boards. The control board is based on DSP chip and CPLD chip, it has enough calculating capability and speed for our operation.

Using the one phase hardware, the concept of the voltage ripple suppression method can already be verified. Fig.4. 9 plots the experimental results of harmonic current elimination method (Example 2) and second order harmonic current injection method (Example 3). For the safety concern, the DC bus voltage rating of those experiment is only 60V. However, the effects of harmonic current control and voltage ripple



reducing can be implemented with this hardware prototype. The voltage ripple with second order injection is around 20 % smaller than that in example 2, which is same as simulation results.

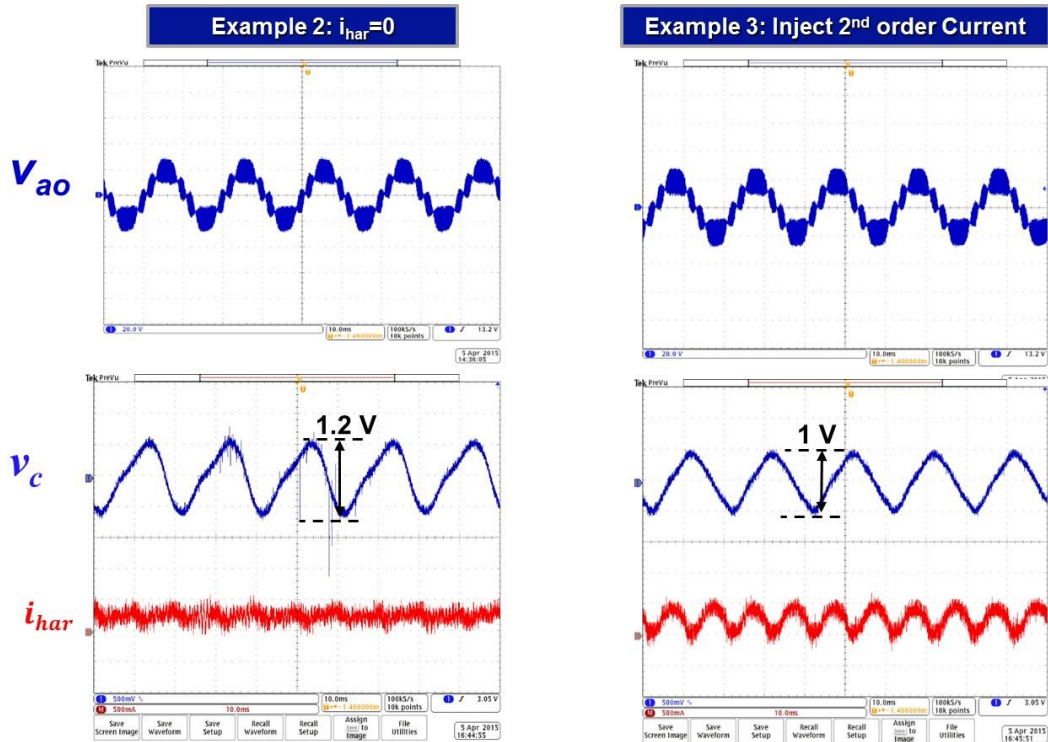


Fig.4. 9 experimental results of example 2 and example 3

With modulation index control and full bridge module, as previous proposed, the capacitor voltage ripple reducing can be improved. Fig.4. 10 plots the experimental result for it. Due to the effect of inductors and other components in the circuit, the results is not as good as simulation. However, when the switching frequency ripple is neglected, the voltage ripple is also significantly reduced.

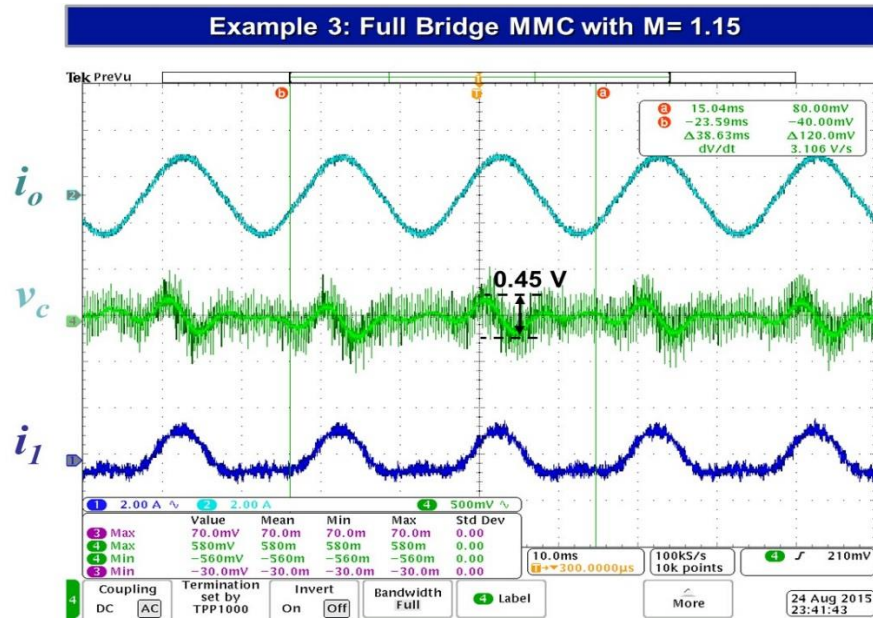


Fig.4. 10 experimental results of modulation index control method

As in Fig.4. 5 shown, there are four controller for this three phase system. One of them is the master controller and the others are slave controllers. When the system works as three phase, it is not as simple as single phase. The communication between phases is important. Therefore, the master and slave controller have different control tasks, showing in TABLE 4. 3

Fig.4. 11 shows three phase scaled down hardware of MMC. Besides the components mentioned previously, there is a sensor board to measure the output voltage and arm current.

TABLE 4. 3 CONTROLLER TASK

	Control task	Measurements	Communication
Master controller	Output Voltage Control	Output Voltage	Average capacitor voltage from slave
	Phase balance control	DC Voltage	Running & Fault status
	Arm balance control	Arm Current	
	Over current & voltage protection		
slave controller	Module balance control	Module Voltage	Voltage reference of each arm from master
	Module protection	Arm Current	Running & Fault status

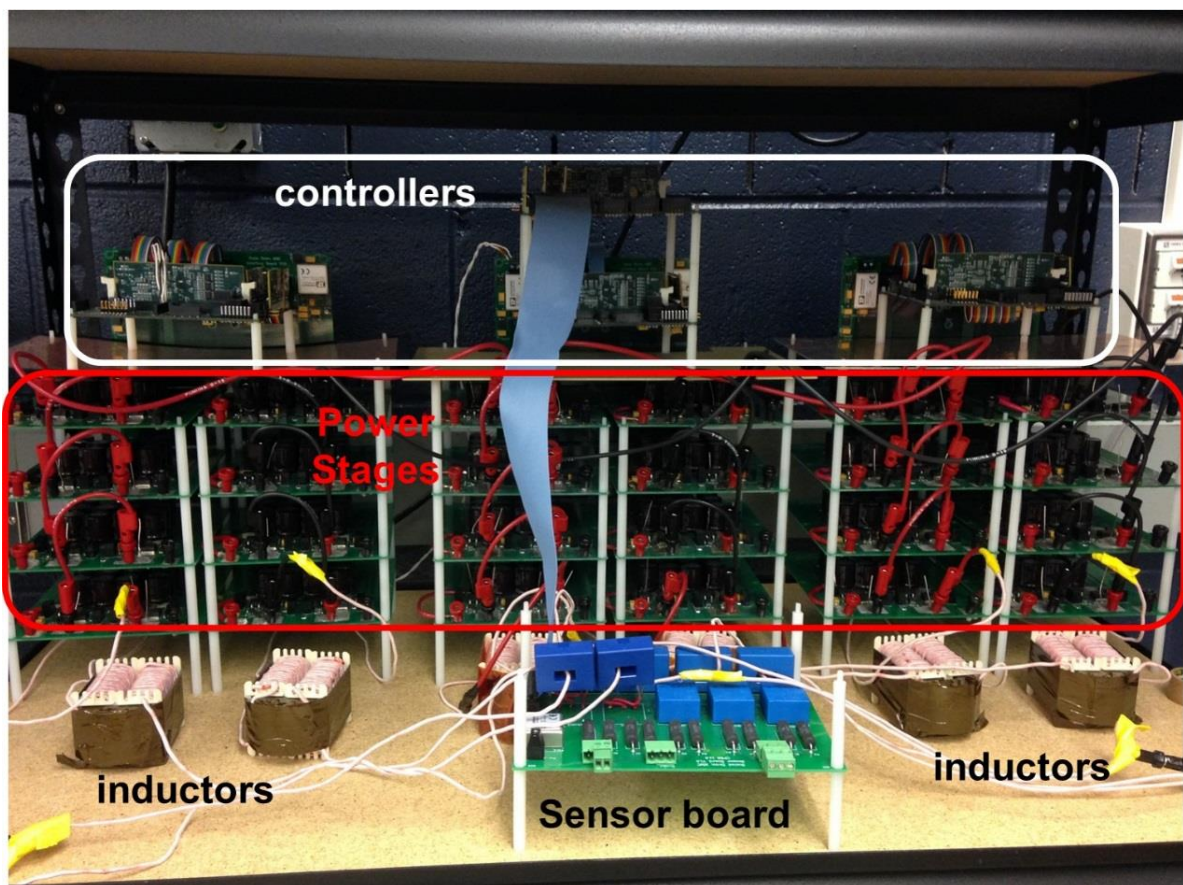


Fig.4. 11 Three phase scaled down hardware of MMC

With this hardware, the concept of voltage ripple reduction control strategies can be verified. In future, it will also help us find out more

---

opportunities of improving the performance of modular multilevel convertor.

---

## Chapter 5 Conclusion and Future Work

### *5.1 Summary and conclusion*

To gain a better understanding of the intricate operations of the modular multi-level converter, this thesis proposes a method of analysis that utilizes both state trajectory analysis and power flow analysis. The flow of the circulating energy of the system is portrayed as state trajectories on a three-dimensional state space and is further simplified to a set of two-dimensional state plans. Subsequently, this method offers a clear portrayal of the energy state within a module and the energy transfer in the system over a line cycle. The method can be effectively used to assess the merits and drawbacks of various control strategies for minimizing capacitor energy storage for each module. The method clearly delineates the energy storage transfer to the load and energy circulating to the sources as well as the energy circulating among modules.

The analysis begins by breaking down the energy components into a series of entities and identifying their association with dc, fundamental line frequency and various harmonics. The flow of the various components of power at the system level are displayed on the state plans with a clear delineation of the power delivered to the load from the circulating energy to the sources, as well as among the modules themselves. The proposed

---

method enables one to gain a better understanding of the working principle of the MMC and offers a simple way to assess the effectiveness of the various control strategies with visual support by portraying its state trajectories on two-dimensional planes.

Moreover, a new control strategy for reducing capacitor voltage ripple is proposed. Controlling modulation index with full bridge module can eliminate the fundamental harmonic voltage ripple, which is the main obstacle of reducing capacitance. The theoretical concept also can be verified on the scaled down hardware.

## ***5.2 Future work***

Basing on the loss evaluation in section 4, we find that the semiconductor loss in modulation index design is around 160% of the original case. Therefore, a new hybrid topology which combines half bridge and full bridge is being explored. From that hybrid topology, we expect a balance between voltage ripple reduction and semiconductor loss

With our control concept, a 3rd harmonic voltage is still left in the module. The next step is to analyze possible injected currents to further reduce the 3rd order capacitor voltage ripple.

---

Utilize the proposed saving capacitance method in MMC-HVDC system, and quantify the effectiveness of the proposed method. A tradeoff between converter loss and saving capacitance would also be analyzed based on CPES double-pulse test results of IGBT.

An optimization design of inductors is also necessary to build a solid fundamental for further research. The optimization design of inductors should include the considerations of protection, THD requirement, loss and cost.

---

## References

---

- [1] Siemens website “High voltage direct current Transmission-Proven Technology for Power Exchange”
- [2] Siemens “Fact Sheet High-voltage direct current transmission (HVDC)”  
May 2014
- [3] K. R. Padiyar, HVDC Power Transmission Systems: Technology and System Interactions. New York/Chichester, U.K.: Wiley, 1990
- [4] J. Arrillaga, High Voltage Direct Current Transmission. London, U.K.: Inst. Electr. Eng., 1998.
- [5] J. Casazza and G. C. Loehr, The Evolution of Electric Power Transmission Under Deregulation: Selected Readings. Piscataway, NJ: IEEE Press, 2000
- [6] B. Andersen, L. Xu, P. J. Horton, and P. Cartwright, “Topologies for VSC transmission,” *Power Eng. J.*, vol. 16, no. 3, pp. 142–150, Jun. 2002.
- [7] L. Xu and V. Agelidis, “VSC transmission system using flying capacitor multilevel converters and hybrid PWM control,” *IEEE Trans. Power Del.*, vol. 22, no. 1, pp. 693–702, Jan. 2007.



---

---

[ 8 ] J. Dorn, H. Huang, and D. Retzmann, "A new multilevel voltagesourced converter topology for HVDC applications," in Proc. CIGRE Conf., 2008, pp. 1–8, paper B4–304.

[9] B. Gemmell, J. Dorn, D. Retzmann, and D. Soerangr, "Prospects of multilevel VSC technologies for power transmission," in Proc. IEEE Transmission and Distribution Conf. Expo., Apr. 2008, pp. 1–16.

[10] S. Allebrod, R. Hamerski, and R. Marquardt, "New transformerless, scalable modular multilevel converters for HVDC-transmission," in Conf. Rec. IEEE PESC, 2008, pp. 174–179.

[11] R. Marquardt "Modular multilevel converter topologies with DCshort circuit current limitation", Proc.8th Int. Power Electron. ECCE Asia Conf., pp.1425 -1431 2011

[12] R. Marquardt "Modular multilevel converter: An universal concept for HVDC-Networks and extended DC-Bus-applications", Proc. Int. Power Electron. Conf., 2010, Jun. 2010

[13] R. Marquardt, A Lesnicar, "New Concept for High Voltage - Modular Multilevel Converter," PESC 2004, Aachen.

---

---

[14] R. Marquardt, A Lesnicar, "A new modular voltage source inverter topology," EPE 2003, Toulouse

[15] H.J. Knaak, " Modular Multilevel Converters and HVDCIFACTS: a success story, " In Conf EPE 2011, Birmingham.

[ 16 ] R.Marquardt, "Stromrichterschaltungenmit verteilten Energiespeichern" German Patent DE 10 103 031/24.01.2001, Jan. 24, 2001.

[17] S. Allebrod, R. Hamerski, and R. Marquardt, "New transformerless, scalable modular multilevel converters for HVDC-transmission," in Proc. IEEE Power Electron. Spec. Conf., Jun. 2008, pp. 174–179.

[18] J. Dorn, H. Huang, and D. Retzmann, "A new multilevel voltage-sourced onverter topology forHVDCapplications," in Proc.Conf. Int. des Grands eseaux Electriques, 2008, pp. 1–8.

[19] K. Kunomura, K. Yoshida, K. Ito, N. Nagayama, M. Otsuki, T. Ishizuka, F. Aoyama, and T. Yoshino, "Electronic frequency converter," in Proc. IEEJ IPEC, 2005, pp. 2187–2191.

---

---

[20] L. Franquelo, J. Rodr'iguez, J. Leon, S. Kouro, R. Portillo, and M. Prats, "The age of multilevel converters arrives," *IEEE Ind. Electron. Mag.*, vol. 2, no. 2, pp. 28–39, Jun. 2008.

[21] J. Rodr'iguez, L. Franquelo, S. Kouro, J. Leon, R. Portillo, M. Prats, and M. Perez, "Multilevel converters: An enabling technology for high-power applications," *Proc. IEEE*, vol. 97, no. 11, pp. 1786–1817, Nov. 2009.

[22] G. Ding, M. Ding and G.Tang "An Innovative Modular Multilevel Converter Topology and Modulation Control Scheme for the first VSC-HVDC project in China", in *Proc. 16th Power Systems Computation Conference (PSCC)*, 14-18 July 2008, Glasgow, United Kingdom.

[23] R. Marquardt and A. Lesnicar "New Concept for High Voltage – Modular Multilevel Converter", *IEEE PESC 2004*, Aachen

[24] S. Allebrod, R. Hamerski and R. Marquardt, "New transformerless, scalable Modular Multilevel Converters for HVDC transmission", *IEEE PESC 2008*, Rhodes.

[25] H. Huang, "Multilevel Voltage Source Converters for HVDC and FACTS Application", *Cigre Colloquium*, Bergen 2009.

---

---

[26] Y. Tang, L. Ran, O. Alatise, and P. Mawby, "Capacitor Selection for Modular Multilevel Converter," in Proc. IEEE ECCE, Pittsburgh, PA, USA, Sep. 2014, pp. 2080-2087.

[27] M. Zhang, L. Huang, W. Yao, and Z. Lu, "Circulating harmonic current elimination of a CPS-PWM based modular multilevel converter with plug-in repetitive controller," IEEE Trans. Power Electron., vol. 29, no. 4, pp. 2083–2097, Apr. 2014.

[28] K. Wang, Y. Li, Z. Zheng, and L. Xu, "Voltage balancing and fluctuation suppression method of floating capacitors in a new modular multilevel converter," IEEE Trans. Ind. Electron., vol. 60, no. 5, pp. 1943–1954, May 2013.

[29] Makoto Hagiwara Hirofumi Akagi, "Control and Experiment of Pulsewidth-Modulated Modular Multilevel Converters" IEEE TRANSACTIONS ON POWER ELECTRONICS, VOL. 24, NO. 7, JULY 2009

[30] V. Agelidis and M. Calais, "Application specific harmonic performance evaluation of multicarrier PWM techniques," in Proc. IEEE Power Electronics Specialists Conf., May 1998, vol. 1, pp. 172–178.

---

---

[31] Kouro, S., Bernal, R., Miranda, H., et al.: ‘High-performance torque and flux control for multilevel inverter fed induction motors’, *IEEE Trans. Power Electron.*, 2007, 22, (6), pp. 2116–2123

[32] Moranchel, M., Bueno, E.J., Rodriguez, F.J., et al.: ‘Implementation of nearest level modulation for modular multilevel converter’. *IEEE 6th Int. Symp. PEDG*, June 2015, pp. 1–5

[33] *IEEE Standard for Floating-Point Arithmetic*, IEEE Std. 754-2008, 29 August 2008

[34] J. Rodriguez, J. S. Lai, and F. Z. Peng, “Multilevel inverters: A survey of topologies, controls, and applications,” *IEEE Trans. Ind. Electron.*, vol. 49, no. 4, pp. 724–738, Aug. 2002.

[35] H. Akagi, S. Inoue, and T. Yoshii, “Control and performance of a transformerless cascade PWM STATCOM with star configuration,” *IEEE Trans. Ind. Appl.*, vol. 43, no. 4, pp. 1041–1049, Jul./Aug. 2007.

[36] M. Zhang, L. Huang, W. Yao, and Z. Lu, “Circulating harmonic current elimination of a CPS-PWM based modular multilevel converter with plug-in repetitive controller,” *IEEE Trans. Power Electron.*, vol. 29, no. 4, pp. 2083–2097, Apr. 2014.

---

---

[37] K. Wang, Y. Li, Z. Zheng, and L. Xu, "Voltage balancing and fluctuation suppression method of floating capacitors in a new modular multilevel converter," *IEEE Trans. Ind. Electron.*, vol. 60, no. 5, pp. 1943–1954, May 2013.